

Online Research @ Cardiff

This is an Open Access document downloaded from ORCA, Cardiff University's institutional repository: <https://orca.cardiff.ac.uk/id/eprint/145148/>

This is the author's version of a work that was submitted to / accepted for publication.

Citation for final published version:

Fernández, Yolanda, Movellan, Julie, Foradada, Laia, Giménez, Vanessa, García-Aranda, Natalia, Mancilla, Sandra, Armiñán, Ana, Borgos, Sven Even, Hyldbakk, Astrid, Bogdanska, Anna, Gobbo, Oliviero L., Prina-Mello, Adriele, Ponti, Jessica, Calzolari, Luigi, Zagorodko, Oleksandr, Gallon, Elena, Niño-Pariente, Amaya, Paul, Alison ORCID: <https://orcid.org/0000-0002-7653-9964>, Schwartz, Simó, Abasolo, Ibane and Vicent, María J. 2022. In vivo Antitumor and ametastatic efficacy of a polyacetal-based paclitaxel conjugate for prostate cancer therapy. *Advanced Healthcare Materials* 11 (7) , 2101544. 10.1002/adhm.202101544 file

Publishers page: <http://dx.doi.org/10.1002/adhm.202101544>
<<http://dx.doi.org/10.1002/adhm.202101544>>

Please note:

Changes made as a result of publishing processes such as copy-editing, formatting and page numbers may not be reflected in this version. For the definitive version of this publication, please refer to the published source. You are advised to consult the publisher's version if you wish to cite this paper.

This version is being made available in accordance with publisher policies.

See

<http://orca.cf.ac.uk/policies.html> for usage policies. Copyright and moral rights for publications made available in ORCA are retained by the copyright holders.



1
2
3
4
5
6
7
8
9
10
11
12
13
14
15
16
17
18
19
20
21
22
23
24
25
26
27
28
29
30
31
32
33
34
35
36
37
38
39
40
41
42
43
44
45
46
47
48
49
50
51
52
53
54
55
56
57
58
59
60
61
62
63
64
65

IN VIVO ANTI-TUMOR AND METASTATIC EFFICACY OF A POLYACETAL-BASED PACLITAXEL CONJUGATE FOR PROSTATE CANCER THERAPY

Yolanda Fernández^{a,b,c}, Julie Movellan^d, Laia Foradada^{a,b,c}, Vanessa Giménez^d, Natalia García-Aranda^{a,b,c}, Sandra Mancilla^{a,b,c}, Ana Armiñán^d, Sven Even Borgos^e, Astrid Hyldbakk^e, Anna Bogdanska^{f,g}, Oliviero L. Gobbo^{h,g}, Adriele Prina-Mello^{f,g}, **Jessica Pontiⁱ, Luigi Calzolariⁱ**, Oleksandr Zagorodko^d, Elena Gallon^d, Amaya Niño-Pariente^d, Alison Paul^j, Simó Schwartz Jr.^{b,c}, Ibane Abasolo^{a,b,c*}, María J. Vicent^{d,*}

^a Functional Validation & Preclinical Research (FVPR), CIBBIM-Nanomedicine, Vall d'Hebron Institut de Recerca (VHIR), Universitat Autònoma de Barcelona (UAB), 08035 Barcelona, Spain

^b Drug Delivery & Targeting Group, CIBBIM-Nanomedicine, Vall d'Hebron Institut de Recerca (VHIR), Universitat Autònoma de Barcelona (UAB), 08035 Barcelona, Spain

^c Networking Research Center on Bioengineering, Biomaterials and Nanomedicine (CIBER-BBN), Barcelona, Spain

^d Polymer Therapeutics Laboratory. Centro de Investigación Príncipe Felipe. Av. Eduardo Primo Yúfera 3, 46012 Valencia, Spain

^e Department of Biotechnology and Nanomedicine, SINTEF Industry, Trondheim, Norway

^f Laboratory for Biological Characterization of Advanced Materials (LBCAM), Trinity Translational Medicine Institute, Trinity College Dublin, Dublin, Ireland

^g Trinity St James's Cancer Institute, Trinity College Dublin, the University of Dublin, Dublin, Ireland

^h School of Pharmacy and Pharmaceutical Sciences, Trinity College Dublin, Ireland

ⁱ **European Commission, Joint Research Centre (JRC), 21027 Ispra, Italy**

^j School of Chemistry, Cardiff University, Main Building, Park Place, Cardiff CF10 3AT, UK

*Corresponding authors:

Ibane Abasolo, Ph.D. Functional Validation & Preclinical Research (FVPR), Passeig Vall d'Hebron 119-129, 08035 Barcelona, Spain. E-Mail: ibane.abasolo@vhir.org

María J Vicent, Ph.D. Polymer Therapeutics Laboratory. Av. Eduardo Primo Yúfera 3, 46012 Valencia, Spain. E-mail: mjvicent@cipf.es

ABSTRACT

1
2 Prostate cancer (PCa), one of the leading causes of cancer-related deaths, currently lacks
3
4 effective treatment for advanced-stage disease. Paclitaxel (PTX) is a highly active
5
6 chemotherapeutic drug and the first-line treatment for PCa; however, conventional PTX
7
8 formulation causes severe hypersensitivity reactions and limits PTX use at high concentrations.
9
10 In the pursuit of high molecular weight, biodegradable, and pH-responsive polymeric carriers,
11
12 we conjugated PTX to a polyacetal-based nanocarrier to yield a *tert*-Ser-PTX polyacetal
13
14 conjugate. *tert*-Ser-PTX conjugate provides sustained release of PTX over two weeks in a pH-
15
16 responsive manner while also obtaining a degree of epimerization of PTX to 7-epi-PTX. Serum
17
18 proteins stabilize *tert*-Ser-PTX, with enhanced stability in human serum vs. PBS (pH 7.4). *In vitro*
19
20 efficacy assessments in PCa cells demonstrated IC₅₀ values above those for the free form of PTX
21
22 due to the differential cell trafficking modes; however, *in vivo* tolerability assays demonstrated
23
24 that *tert*-Ser-PTX significantly reduced the systemic toxicities associated with free PTX
25
26 treatment. *tert*-Ser-PTX also effectively inhibited primary tumor growth and hematologic,
27
28 lymphatic, and coelomic dissemination, as confirmed by *in vivo* and *ex vivo* bioluminescence
29
30 imaging and histopathological evaluations in mice carrying orthotopic LNCaP tumors. Overall,
31
32 our results suggest the application of *tert*-Ser-PTX as a robust anti-tumor/antimetastatic
33
34 treatment for PCa.
35

KEYWORDS

36
37 Nanomedicine, polymer-drug conjugates, paclitaxel, prostate cancer, polyacetals, anti-tumor
38
39 efficacy, pH-responsiveness.
40
41
42
43
44
45
46
47
48
49
50
51
52
53

INTRODUCTION

1
2 Metastasis, the last stage of cancer progression, represents a sequential series of
3
4 interrelated steps, including local invasion, intravasation, survival in the bloodstream and lymph,
5
6 extravasation, and growth within a secondary organ and the cause of most cancer-related
7
8 death.^[1] Therefore, the formation of incurable metastases represents a significant problem in
9
10 cancer treatment rather than the eradication of the primary tumor itself. While early-stage
11
12 prostate cancer (PCa) is treatable, with a five-year survival rate exceeding 90%, nearly 30% of
13
14 men treated by radical prostatectomy suffer from disease relapse, and their prognosis remains
15
16 poor.^[2-4] Androgen ablation represents a commonly used therapy for advanced metastatic
17
18 PCa,^[5] to which most patients initially respond; however, most patients eventually relapse and
19
20 succumb to androgen-independent PCa and metastasis. The design of new therapeutic
21
22 strategies to improve the anti-tumor and antimetastatic efficacy of PCa drug treatments
23
24 represents an essential step to ensure adequate disease management.^[6]

25
26 Nanomedicines have emerged as exciting new therapeutic modalities for unmet clinical
27
28 needs, and in this study, we focused on the potential of Polymer Therapeutics, particularly
29
30 polymer-drug conjugates (PDCs), for the treatment of advanced metastatic PCa.^[7] PDCs are
31
32 defined as macromolecular complexes in which a drug is covalently bound to a water-soluble
33
34 polymeric carrier.^[8] Compared to conventional small molecule-based therapies, PDCs have
35
36 several advantages for cancer therapy, including i) enhanced aqueous solubility, ii) higher drug
37
38 loading capacity, iii) prolonged blood circulation times and, therefore, improved bioavailability
39
40 and biodistribution via the so-called enhanced permeability and retention (EPR) effect,^[9] and
41
42 consequently, iv) reduced toxicity for healthy tissues and v) increased anti-tumor efficacy.^[10]

43
44 The design of improved biodegradable polymeric carriers that exploit EPR-mediated
45
46 tumor targeting and/or controlled drug release at a specific loci, represents an ongoing
47
48 multidisciplinary challenge. Biodegradable polymers such as polyacetals^[11,12] constitute
49
50 promising candidates for the design of PDCs as they display pH-dependent degradation; while
51
52 they remain stable at pH 7.4, polyacetals rapidly degrade in response to the acidic environments
53
54 encountered in endosomes and lysosomes (e.g. pH 5-5.5).^[11,13] *In vitro* and *in vivo* studies using
55
56 polyacetals have previously confirmed a lack of toxicity and low uptake by the liver and spleen
57
58 combined with enhanced blood circulation times.^[11]

59
60 The microtubule-interfering agent paclitaxel (PTX) is a clinically well-established and
61
62 highly effective chemotherapeutic drug used to treat advanced tumors, including prostate,
63
64 breast, ovarian, and non-small cell lung cancer. In addition to anti-neoplastic activity, PTX
65

1 exhibits anti-angiogenic and pro-apoptotic effects at low doses;^[14-16] however, observed severe
2 side effects limit the application of PTX. Given its hydrophobic nature, the clinical application of
3 PTX requires solubilization in Cremophor EL® or ethanol, which prompt hypersensitivity
4 reactions.^[17] PTX also displays inherent severe side effects, including neurotoxicity.^[18] Additional
5 limitations of PTX include a poor pharmacokinetic profile (short half-life, low selectivity), which
6 leads to a negligible level of PTX reaching the tumor site and the development of drug resistance
7 due to the nature of PTX as a substrate for efflux pumps.^[19]

8
9
10
11
12
13 The development of an albumin-based PTX nanoparticle (Abraxane™ - ABI-007, Celgene
14 Corporation) represents a successful approach for PTX delivery. The United States Food and
15 Drug Administration (FDA) approved Abraxane in 2004 for the treatment of breast cancer after
16 the failure of combination chemotherapy for metastatic disease or relapse within six months of
17 adjuvant chemotherapy. In this formulation, PTX is physically complexed within the Abraxane
18 nanoparticle, leading to the enhanced solubility of PTX and the avoidance of harmful solubilizing
19 agents.^[20] Even given the success of Abraxane, the conjugation of PTX to a polymeric carrier
20 might offer further pharmacological advantages. Conjugation of PTX to N-(2-hydroxypropyl)
21 methacrylamide (HPMA), a non-biodegradable copolymer, led to improved pharmacokinetics
22 and promising anti-tumor efficacy;^[21] however, this strategy failed at the clinical stage due to
23 the premature release of PTX in the circulation, producing a similar toxicity profile to free PTX.
24 Cell Therapeutics Inc. (Seattle, USA) took a different approach and conjugated PTX to
25 polyglutamic acid (a biodegradable polymer) to create OPAXIO™, which displayed clinical
26 benefits compared to free PTX when used alone or in combination with radiotherapy or other
27 small drugs such as cisplatin.^[22-24]

28
29
30
31
32
33
34
35
36
37
38
39
40 In this study, we synthesized and exhaustively characterized (demonstrating batch-to-
41 batch reproducibility and endotoxin-free large-scale synthesis) a pH-responsive polyacetal-PTX
42 conjugate (*tert*-Ser-PTX) to understand conjugate behavior at the cellular and whole-organism
43 levels. Polyacetal conjugation inhibited the early release of PTX in the bloodstream but
44 supported the pH-triggered release of PTX after the EPR-mediated accumulation within tumors.
45
46 Encouragingly, *tert*-Ser-PTX demonstrated robust anti-tumor efficacy in primary tumors and
47 significantly inhibited metastatic dissemination. Overall, we hypothesize that the conjugation of
48 PTX to a pH-responsive polyacetal carrier will offer enhanced clinical benefits to PCa patients by
49 enabling a low-dose clinical regime, controlled release of the drug, and a reduction in harmful
50 side effects.
51
52
53
54
55
56
57
58
59

MATERIAL AND METHODS

1. Synthesis and characterization of *tert*-polyacetal-paclitaxel (*tert*-Ser-PTX)

1.1 Synthesis of polyacetal *tert*-FmocSerinol

PEG₄₀₀₀ (5 g, 1.25 mmol) and *p*-toluenesulfonic acid (pTSA) (8 mg, 0.0464 mmol) were first azeotropically distilled from toluene (40 mL) at 150°C for 2 h. Then, Fmoc-serinol (472 mg, 1.53 mmol) in anhydrous tetrahydrofuran (THF) was added, and the mixture was dried under a high vacuum. The mixture was re-dissolved in anhydrous THF, and di(ethylene glycol) divinyl ether (DEGDVE) (456 μL, 2.78 mmol) was added dropwise. The mixture was allowed to stir for 3 h in the dark at room temperature. 1 mL of triethylamine was added to the reaction mixture under vigorous stirring. After 10 min, the mixture was precipitated into hexane (400 mL), decanted, washed with another 400 mL of hexane, and then collected by vacuum filtration.

Yield: 90%. ¹H-NMR (Acetone-d₆, 300 MHz) δ (ppm) 0.85-0.90 (t, J = 0.9 Hz, 2.5H), 1.22-1.27 (12H, m, PEG-acetal CH₃), 3.35-3.88 (204H, m, PEG CH₂, DEG CH₂, Serinol CH₂), 4.24 (1H, m, Fmoc Ar-CH-CH₂-), 4.36 (2H, m, Fmoc Ar-CH-CH₂-), 4.74-4.77 (3H, m, acetal CH), 7.33-7.41 (4H, m, ArHFmoc), 7.71 (2H, m, ArHFmoc), 7.85 (2H, m, ArHFmoc).

1.2 Fmoc Deprotection

tert-Fmoc Serinol was dissolved in a flask using 20% piperidine/acetonitrile (40 mL) as the deprotection reagent, and the reaction mixture was stirred for 1 h at room temperature. Then, the crude product was precipitated once in diethylether (400 mL) and twice in hexane (400 mL). The solid was redissolved in a minimum amount of acetone between each precipitation. Finally, *tert*-Serinol was dried under a high vacuum for 1 h. Yield: 90 %.

tert-FmocSerinol: ¹H-NMR (Acetone-d₆, 300 MHz) δ (ppm) 1.22-1.33 (m, 3H, PEG-acetal -CH₃), 3.35-3.85 (m, 67H, PEG DEG -CH₂, Serinol-CH₂), 4.80 (m, 1H, PEG-acetal -CH).

1.3 Synthesis of 2'-succinyl-paclitaxel (PTX_{COOH})

PTX (300 mg, 0.35 mmol) and succinic anhydride (450 mg, 4.5 mmol) were dissolved in anhydrous pyridine (5 mL) and stirred under a nitrogen atmosphere at room temperature for 4 h. Then, pyridine was evaporated under high vacuum, and the crude product was washed with water and filtered. The white solid obtained was recrystallized in acetone/water and freeze-dried.

Yield: 64%. *PTX*_{COOH}: ¹H-NMR (Acetone-d₆, 300 MHz) δ (ppm) 1.20 (s, 3H, -CH₃), 1.22 (s, 3H, -CH₃), 1.67 (s, 3H, -CH₃), 1.96 (s, 3H, -CH₃), 2.17 (s, 3H, -CH₃), 2.47 (s, 3H, -CH₃), 2.64 (d, 2H, CH₂-suc), 2.71 (d, 2H, CH₂-suc), 3.89 (m, 2H, -CH₂), 4.20 (m, 2H, -CH₂), 4.45 (m, 1H, -CH), 4.98 (m, 1H,

1
2
3
4
5
6
7
8
9
10
11
12
13
14
15
16
17
18
19
20
21
22
23
24
25
26
27
28
29
30
31
32
33
34
35
36
37
38
39
40
41
42
43
44
45
46
47
48
49
50
51
52
53
54
55
56
57
58
59
60
61
62
63
64
65

-CH), 5.57 (d, 1H, -CH-suc), 5.70 (d, 1H, -CH), 5.98 (m, 1H, -CH), 6.17 (t, 1H, -CH), 6.43 (s, 1H, -CH), 7.31-7.70 (m, 11H, ArH), 7.88 (d, 2H, ArH), 8.14 (d, 2H, ArH), 8.45 (d, 1H, NH).

1.4 Synthesis of *tert*-Ser-PTX

tert-Ser-PTX was obtained through a reaction between PTX_{COOH} (0.13 g, 0.134 mmol), *tert*-Serinol (2.13 g), and 4-(4,6-Dimethoxy-1,3,5-triazin-2-yl)-4-methylmorpholinium tetrafluoroborate (DMTMM-BF₄) (50 mg, 0.152 mmol) using 15-20 ml anhydrous N,N-dimethylformamide (DMF) as a solvent. PTX_{COOH} and DMTMM-BF₄ were first poured into a Schlenk flask and dried under a high vacuum for 1 h and were then dissolved in DMF (3 mL) while stirring under a nitrogen atmosphere protected from the light. *tert*-Serinol was added after 10 min using DMF (15 mL) to dissolve completely. The pH of the reaction mixture was adjusted to 8 using N,N-diisopropylethylamine (DIEA). After 16 h, the crude product was precipitated in diethylether (200 mL) and collected by vacuum filtration. The white solid obtained was redissolved using a minimum amount of acetone and dialyzed against acetone using a regenerated cellulose membrane (molecular weight cutoff [MWCO] 3.5 kDa).

Yield: 85%. ¹H-NMR (Acetone-d₆, 300 MHz) δ (ppm) 1.19-1.34 (m, 76H, -CH₃ PEG acetal, 2 -CH₃ PTX), 1.66 (s, 3H, -CH₃ PTX), 1.97 (s, -CH₃ PTX), 2.19 (s, 3H, -CH₃ PTX), 2.45 (s, 3H, -CH₃ PTX), 2.53 (m, 5H, PTX), 3.34-3.84 (m, 1627H, PEG DEG CH₂, Serinol-CH₂), 4.10-4.17 (m, 3H, PTX), 4.42 (m, 1H, -CH PTX), 4.73-4.79 (m, 21H, -CH PEG-acetal), 4.95-4.98 (d, 1H, 5.0 Hz, -CH PTX), 5.53 (d, 1H, 5.5 Hz, CH PTX), 5.70 (d, 1H, 5.7 Hz, -CH PTX), 5.93-5.98 (t, 1H, 5.9 Hz, -CH PTX), 6.11-6.18 (t, 1H, 6.1 Hz, -CH PTX), 7.07 (m, 1H, ArH PTX), 7.31 (m, 1H, ArH PTX), 7.45-7.70 (m, 11H, ArH PTX), 7.91 (m, 2H, ArH PTX), 8.13 (d, 2H, 8 Hz, ArH PTX), 8.4 (m, 1H, NH PTX).

1.5 Physicochemical characterization of *tert*-Ser-PTX

Physicochemical characterization of *tert*-Ser-PTX involved 1D and 2D NMR, dynamic light scattering (DLS), transmission electron microscopy (TEM), size exclusion chromatography (SEC), reversed-phase liquid chromatography with electrospray positive ionization tandem mass spectrometry (LC-MS/MS) of PTX and the epimer 7-epi-PTX, and small-angle neutron scattering (SANS) measurements. Please see the **Supporting Information** for further details.

1.5.1. Determination of total drug loading and free drug content by LC-MS/MS.

Reconstituted *tert*-Ser-PTX was incubated at 37°C in phosphate-buffered saline (PBS) adjusted to pH 7.4, 5.5, and 4.0 at a target concentration of 2 μg mL⁻¹ conjugated PTX based on the PTX loading determination by NMR (8% w/w PTX). Sampling was performed at the following times: 0 h, 1 h, 4 h, one day, two days, four days, one week, and two weeks. Organic solvent (acetonitrile) was added at 9 volumes (1+9) to solubilize the released PTX, which was

1 subsequently quantified by LC-MS/MS. As a degradation control, free PTX at 2 $\mu\text{g mL}^{-1}$ was
2 incubated under identical conditions.
3

4 For the forced degradation study, 100 $\mu\text{g mL}^{-1}$ of free PTX or PTX equivalent (*tert*-Ser-PTX,
5 theoretical PTX loading 8 % w/w) was incubated in 4M H_2SO_4 at 90°C overnight. After 100x
6 dilution in water, the samples were analyzed by LC-MS/MS to quantify benzoic acid.
7
8
9

10 **1.6 Drug release in simple and complex media**

11 **1.6.1 pH-dependent degradation**

12 Polyacetals (3 mg mL^{-1}) were incubated at 37°C in PBS at pH 5.5, 6.5, and 7.4 for twenty
13 days. 100 μL samples for high-performance liquid chromatography (HPLC) analysis were isolated
14 at various time points (0, 8 h, and then every 24 h) until complete degradation. Before analysis,
15 the pH of acidic samples was neutralized with ammonium formate buffer (0.1 M, 100 μL for pH
16 5.5 and 50 μL for 6.5) to stop any further degradation, and concentrations were normalized with
17 PBS (100 μL PBS were added to the samples of pH 7.4 and 50 μL to the sample of pH 6.5). Then,
18 samples were directly analyzed by reversed-phase HPLC (RP-HPLC), using a C18 LiChroSpher 100
19 column (5 μm , 15 cm length), with the UV detector set at $\lambda=280\text{ nm}$ with a flow rate of 1 mL min^{-1} ,
20 20 μL injection. Eluent A was H_2O and eluent B was acetonitrile. Estradiol was used as an HPLC
21 internal reference standard; 100 μL of a 10 $\mu\text{g mL}^{-1}$ stock solution was added to each sample.
22 The elution was performed by the following gradient: from 35% B to 80% B over 20 min (PTX
23 retention time: 7 min). A calibration curve of PTX was used to quantify the total PTX release from
24 the conjugates by HPLC.
25
26
27
28
29
30
31
32
33
34
35

36 **1.6.2 Serum stability**

37 Polyacetals (3 mg mL^{-1}) were incubated at 37°C in freshly extracted serum from Wistar
38 rats for up to 24 h. Samples of 100 μL were collected at regular intervals of time. 10 μL of 100
39 $\mu\text{g mL}^{-1}$ solution of estradiol in methanol (internal standard) and 135 μL of acetonitrile were
40 added to each sample to precipitate serum proteins. Following centrifugation (14,000 rpm, 5
41 min), supernatants were analyzed by HPLC (gradient 35% to 80% acetonitrile/water, 20 min, 20
42 μL injection).
43
44
45
46
47
48

49 Additional studies were performed by LC-MS/MS. Free PTX and *tert*-Ser-PTX were
50 incubated at 37°C for up to two weeks in the following matrices: i) PBS, pH 7.4; ii) HepG2 cell
51 culture medium (unbuffered) with 10% fetal bovine serum (FBS); iii) RPMI cell culture medium
52 (buffered at pH 7.4); and iv) human plasma, pH buffered at 7.4 with 50mM HEPES. 0.1% w/v
53 sodium azide was added to all samples to prevent microbial growth. All incubations were
54 performed in triplicates in 96-well-plates where every plate constituted one sampling time.
55
56
57
58
59

1 Sampling was performed at the following times: 0 h, 1 h, 4 h, one day, two days, four days, one
2 week, and two weeks. Three PTX concentrations levels were studied; 0.5, 2, and 20 $\mu\text{g mL}^{-1}$, of
3 which the 2 $\mu\text{g mL}^{-1}$ concentration is closely based on PTX plasma concentrations used in the
4 clinic. For the *tert*-Ser-PTX formulation, these target PTX concentrations were used to calculate
5 the amount of prodrug added, based on the previously measured drug loading (6.8 w/w %). LC-
6 MS/MS quantified PTX and 7-epi-PTX after adding nine volumes of acetonitrile, which solubilizes
7 the PTX (from precipitation and protein binding) and simultaneously precipitates proteins. The
8 free drug was separated by centrifugal ultrafiltration (regenerated cellulose membrane, MWCO
9 10 kDa) in well-plate format at 2,000 g for 5 min.

16 2. *In vitro* efficacy studies

17 2.1 Cells

21 PCa androgen-dependent (LNCaP.Fluc2) and -independent (PC3) cell lines^[25] were used
22 for cytotoxicity assays. LNCaP.Fluc2 PCa cells were obtained from PerkinElmer (Waltham, MA,
23 USA) and PC3 cells from the American Type Culture Collection (Rockville, MD, USA). Briefly,
24 LNCaP.Fluc2 cells were cultured in DMEM medium and PC3 cells in RPMI 1640 medium
25 (Invitrogen, Carlsbad, CA, USA). All media were supplemented with 10% heat-inactivated FBS
26 (Lonza, Verviers, Belgium), penicillin (100 U mL⁻¹), streptomycin (100 $\mu\text{g mL}^{-1}$), and fungizone
27 (250 ng mL⁻¹) (Invitrogen). LNCaP.Fluc2 overexpressed firefly luciferase for *in vivo*
28 bioluminescence imaging (BLI) monitoring, and reporter expression was maintained in cell
29 culture with 500 $\mu\text{g/mL}$ of geneticin (Invitrogen). Cells were maintained in a humid atmosphere
30 at 37°C with 5% CO₂.

31 2.2 *In vitro* cytotoxicity

32 The *in vitro* cytotoxicity of polyacetals was evaluated using the 3-[4,5-dimethylthiazol-2-yl]-
33 2,5-diphenyltetrazolium bromide (MTT) method after 72 h incubation.^[26–28] Cells were treated
34 with *tert*-Ser-PTX or free PTX with final doses ranging from 0.000004 to 40 $\mu\text{g mL}^{-1}$ (PTX
35 equivalents).

36 3. *In vivo* efficacy studies

37 All *in vivo* efficacy studies were performed using the NANBIOSIS Singular Scientific
38 Technological Infrastructures at the *In vivo* Experimental Platform of the Functional Validation
39 & Preclinical Research (FVPR) area of the Bioengineering, Biomaterials and Nanomedicine
40 Networking Biomedical Research Centre (CIBER-BBN) in Barcelona, Spain.
41 (<http://www.nanbiosis.es/unit/u20-in-vivo-experimentalplatform/>)

3.1 Animals

Biodistribution and repeated-maximum tolerated dose (r-MTD) assays were performed using C57BL/6 mice (sourced from Envigo Laboratories, UK and were bred on-site at Trinity College Dublin). Efficacy assays were performed with eight-week-old male NOD-SCID mice (Charles River Laboratories, Inc., Barcelona, Spain). All animals were housed in individually ventilated cage units and maintained under pathogen-free conditions. Food and water were provided *ad libitum*. Specific pathogen-free conditions were employed during the surgery and the follow-up for the animals. The animals were euthanized for necropsy by cervical dislocation after sedation. The experimental protocols employed in this study were approved by the local Animal Research Ethics Committee and Health Products Regulatory Authority (HPRA, ref. AE19136 P073), in accordance with the guidelines of the Animal Ethics Committee Trinity College Dublin, Ireland and Vall d'Hebron's Animal Experimentation Ethical Committee (CEEA, 53/12), Spain and the European Council Directive 1986 (86/806/EEC). Throughout the study, the use and treatment of animals were performed within the Three R's guidelines for ethical animal testing.

Mice were housed in groups and kept under standard housing conditions at a constant temperature ($20 \pm 2^\circ\text{C}$) and standard lighting conditions (cycles of 12 hours light: 12 hours dark). Food and water were available *ad libitum*.

3.2 Biodistribution, Repeated-Maximum Tolerated Dose of *tert*-Ser-PTX, and Tolerability Studies

For the *in vivo* safety investigation, the biodistribution of PTX after single intravenous (i.v.), subcutaneous (s.c.), and intraperitoneal (i.p.) administrations of *tert*-Ser-PTX (20 mg/kg in PTX equivalents) was analyzed in C57BL/6 mice ($n = 4/6$ per group). Quantification of PTX and 7-epi-PTX by LC-MS/MS was carried out in tissue samples collected 24 h post-injection, after enzymatic digestion of organs and precipitation of protein/extraction with acetone.

Repeated dose MTD (r-MTD) analysis was carried in C57BL/6 mice (male and female, $n = 4$ per group and sex) receiving ten daily s.c. injections at 40 mg/kg or the corresponding volume of the vehicle (PBS). Behavior, physical appearance, and weight were monitored and scored to evaluate any visible adverse effects (no observable effect level; NOEL) for 24 days (10 days of treatment plus 14-day follow-up). Different organs (e.g. liver, lung, kidney, spleen and heart) were collected at the experimental endpoint, fixed in formalin, and processed for histological analysis as described in Section 3.5.

1 Tolerability studies in NOD-SCID mice with orthotopic LNCaP tumors (see below) were
2 conducted before efficacy studies following the same treatment schedule. In detail, mice (7 to
3 9 mice per group) were treated with PBS, PTX, or *tert*-Ser-PTX at a dose of 15 PTX/kg by i.v.
4 administration three times a week followed by a rest week followed by the re-initiation of the
5 treatment for up to a total of 3 treatment-rest cycles. Weight loss, physical appearance, and
6 response to stimuli were monitored during treatment, and animals were euthanized if they
7 reached the humane endpoints defined by the Animal Experimentation Ethics Committee. At
8 the experimental endpoint, blood samples were collected by cardiac puncture in EDTA-
9 containing tubes (Sarstedt) to evaluate clinical biochemical parameters in the Servei de
10 Veterinària Clínica of the Universitat Autònoma de Barcelona.

11 3.3 Orthotopic prostate model

12 LNCaP.Fluc2 (1×10^6) cells in 30 μ L sterile PBS were inoculated into the prostate of NOD-
13 SCID mice. The prostate of anesthetized mice was exteriorized through a laparotomy, and cells
14 were injected into the dorsal prostate lobes using a 30-gauge needle attached to an insulin
15 syringe. A well-localized bleb within the injected prostate lobe indicated a technically
16 satisfactory injection. The prostate was washed with saline, returned to the abdominal cavity,
17 and the abdominal wound closed by suturing. During pretreatment, body weight, physical
18 condition, and tumor palpation were measured twice a week. Tumor growth was indirectly
19 monitored through tumor BLI using the noninvasive IVIS[®] Spectrum imaging system. Mice
20 displaying successful prostatic injection of LNCaP.Fluc2 cells were imaged every two weeks with
21 ventral and dorsal views for up to two months. The tumor bioluminescence was quantified over
22 time to determine orthotopic prostate tumor growth in the abdominal cavity. Once the tumors
23 reached a median tumor bioluminescent intensity of $\sim 1.60 \times 10^7$ photons per second (ph s^{-1})
24 (range 1.50×10^6 to $1.60 \times 10^8 \text{ ph s}^{-1}$), mice were randomized into two groups according to their
25 tumor bioluminescent signal. Randomized mice ($n=9$ per group) were treated with the test
26 conjugate at 15 mg PTX/kg by i.v. administration three times a week followed by a rest week
27 followed by the re-initiation of the treatment. On administration days, the bodyweight profile
28 of the experimental groups was monitored before dosing the animals. The animals were
29 administered with treatments only if the mean weight loss of the group was $> 5\%$. During
30 treatment, supervision of the animals was performed every 24 h. Clinical observations recorded
31 included changes in skin, eyes, mucous membranes, alterations in respiratory pattern, behavior,
32 posture, response to handling, and the presence of abnormal movements. Bodyweight and
33 tumor palpation were measured twice a week. Tumor bioluminescent intensity was visualized
34 and quantified once a week for seven weeks. Moreover, the animals were imaged to monitor

1 the metastatic development of other tissues from the dorsal and ventral mouse views. At
2 termination (24 h after the last administration), animals were euthanized by cervical dislocation
3 and subjected to gross necropsy comprising the macroscopic evaluation of all the external body
4 orifices and the examination of the cranial, abdominal, thoracic cavities, and contents. Prostate
5 tumors, lungs, lymph nodes (mesenteric, peripancreatic, and perirenal), and diaphragm were
6 collected. Tumor and metastases were evaluated by *ex vivo* BLI monitoring before the
7 histological analyses.
8
9

10 11 12 13 **3.4 Bioluminescence imaging**

14
15 In vivo and ex vivo BLI was performed with the IVIS® Spectrum Imaging System, and
16 images and measurements of bioluminescent signals were acquired and analyzed using the
17 Living Image® 4.3.1 software (PerkinElmer). The in vivo and ex vivo BLI techniques were
18 developed following procedures previously described in our group.^[29]
19
20

21
22 For *in vivo* BLI, animals were administered 150 mg/kg of D-luciferin (Promega Biotech
23 Ibérica S.L., Spain) in sterile PBS by i.p. injection and anesthetized using 1-3% isoflurane (Abbott
24 Laboratories, IL, USA). Five mice were imaged simultaneously, and imaging settings were set
25 depending on the bioluminescent signals of the orthotopic tumors or metastatic lesions. We
26 imaged our model at a 5–25 min range after D-luciferin injection. The brightest abdominal
27 signals were shielded to detect and quantify weaker signals in the thoracic region. Light emitted
28 from the bioluminescent cells was detected *in vivo* by the IVIS® Spectrum, digitalized, and
29 electronically displayed as a pseudo color overlay onto a grayscale animal image. Regions of
30 interest from images were drawn automatically (threshold = 20%, lower limit = 1.0, and
31 minimum size = 20) around the bioluminescent signals and quantified in ph s^{-1} .
32
33

34
35 For *ex vivo* BLI, mice were euthanized 5-10 min after D-luciferin administration, and
36 tissues of interest were excised, incubated in $300 \mu\text{g mL}^{-1}$ D-luciferin solution, imaged, and
37 quantified as described above. BLI images are set at the same pseudo color scale in the
38 associated figures to show relative bioluminescent changes between different treatment
39 groups.
40
41

42 43 44 45 46 **3.5 Histopathology**

47
48 Immediately after **euthanasia**, organs and tissues were cleaned with PBS, preserved in 4%
49 formaldehyde solution, and then processed for histological analyses. All tissues were paraffin-
50 embedded, sectioned, and stained with hematoxylin and eosin (**H&E**). All sections were assessed
51 by experienced histopathologist at Trinity College Dublin.
52
53
54
55
56
57
58
59

4. Statistical analysis

The mean or median BLI intensities and corresponding standard errors of the mean (SEM) were determined and plotted. Non-linear regression plots were used to describe the relationship between BLI intensity and time after treatment. A non-parametric Mann-Whitney test was applied for peer comparisons in prostate weight and *ex vivo* bioluminescent data. The significance threshold was established at $p < 0.05$, and significance levels were schematically assigned * ($0.01 \leq p < 0.05$), ** ($0.001 \leq p < 0.01$), *** ($0.0001 \leq p < 0.001$) or **** ($p < 0.0001$). All the analyses and graphs were performed using GraphPad Prism 5 software (GraphPad, San Diego).

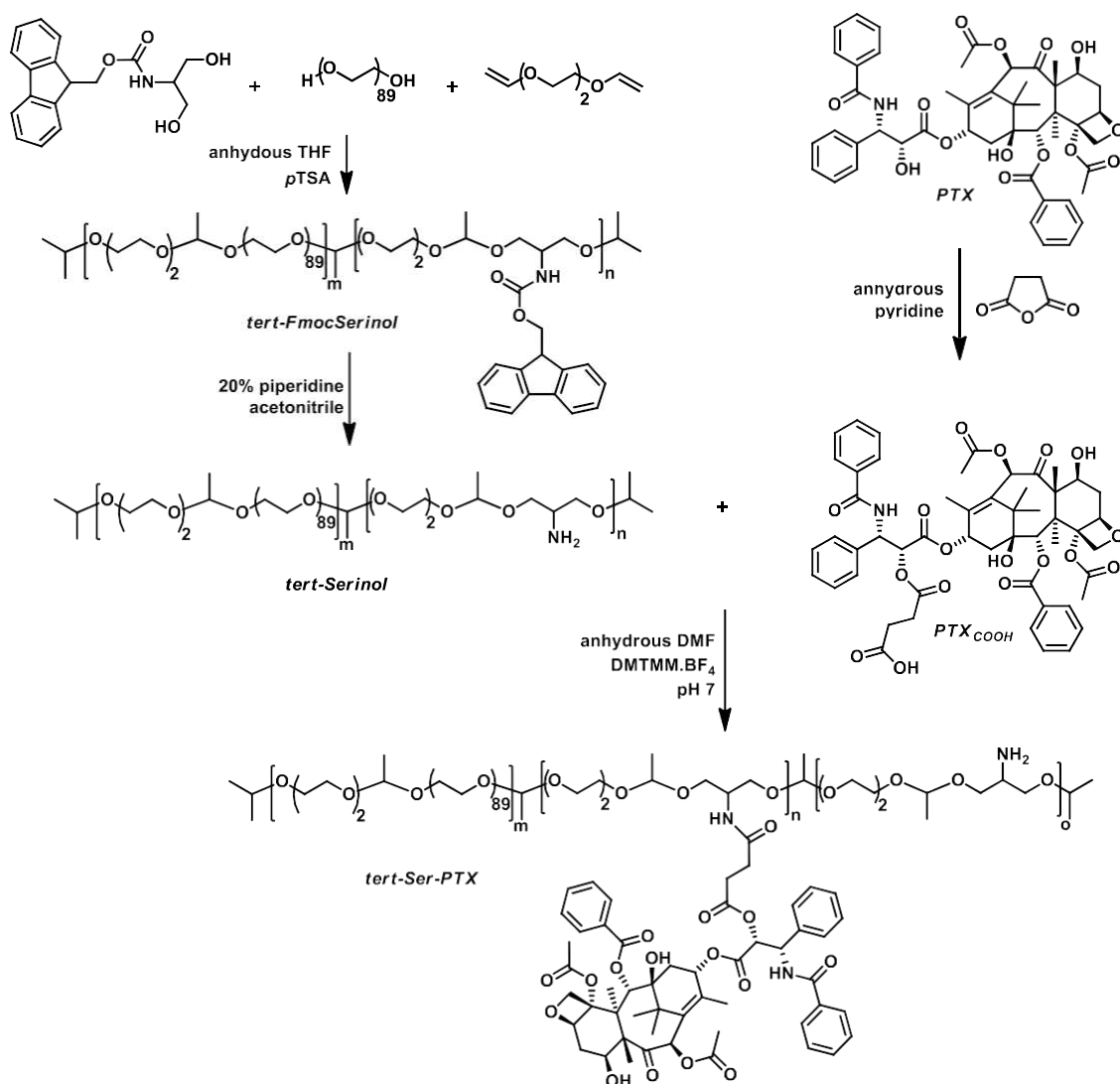
RESULTS AND DISCUSSION

1. Synthesis and characterization of *tert*-Ser-PTX

We incorporated PTX within the sidechains of a pH-susceptible biodegradable polymer to prepare a water-soluble polyacetal-PTX conjugate: *tert*-Ser-PTX (**Table 1**) and then compared the efficacy and potential toxicity to free PTX in an *in vivo* orthotopic LNCaP.Fluc2 PCa model. We prepared the *tert* structure using a simple one-pot synthetic procedure, as previously described.^[11] In brief this uses serinol moieties as co-monomers during the polymerization reaction, forming part of the polymer main chain in a random manner. Incorporated serinol moieties offer new anchoring positions to incorporate PTX in a second step. Before conjugation, we modified the PTX molecule with succinic anhydride to generate 2'-succinyl-PTX. We established a synthetic protocol at the 10-g scale with high batch-to-batch reproducibility (**Scheme 1 and Supplemental Information, Table S1**).

We adopted complementary characterization techniques of incremental complexity to evaluate size distribution, Z potential, morphology, drug loading, drug release in complex media, and protein binding. Firstly, the characterization of polymers by ¹H-NMR ensured acetal bond formation and the correct insertion of Fmoc-serinol in the main polymer chain. The peaks corresponding to the -CH- of acetal groups appear at 4.77 ppm when the acetal bond lies next to an ethylene glycol moiety (**Figure 1a**). We found evidence for the esterification site of 2'-succinyl-PTX through the shift of the signal corresponding to C2' protons of PTX from 4.8 ppm to 5.5 ppm for the succinoylated molecule. We also observed a new set of peaks due to the -CH₂-CH₂- protons of the succinyl moiety at 2.64 ppm and 2.76 ppm. The ¹H-NMR spectrum of the *tert*-Ser-PTX confirmed the formation of an amide bond between the *tert*-Ser conjugate and the 2'-succinyl-PTX by the presence of the peaks due to PTX protons after polymer purification.

We calculated the total PTX loading by integrating the ¹H-NMR of the characteristic peaks of PTX (7.46-8.49 ppm) corresponding to fifteen protons (**Figure S1**), which we determined to be 8 % w/w. A more exhaustive analytical assessment by LC-MS/MS (**Figure 1b** and **Figure S1**) provided a figure of 6.8% w/w PTX total loading, with less than 1.5% free drug not bound to the polymer (**Table 1**). LC-MS/MS constitutes an orthogonal measurement principle to NMR, providing independent verification and ensuring confidence in the challenging analysis of polymeric prodrugs. LC-MS/MS is highly suitable for drug loading measurements, even in complex biological matrices, due to its sensitivity, selectivity, and specificity.



Scheme 1. Synthetic approach for the preparation of *tert*-Ser-PTX.

The formation of the *tert*-Ser-PTX conjugate requires the covalent bonding of PTX to the polyacetal carrier. Since LC-MS/MS is an analytical technique based on the drug's molecular properties, we adapted the standard operating procedures to measure drug loading, free vs.

bound drug fractions, and drug release rates. These parameters can be measured in the same experimental setup by following the free drug concentration as a function of time and the buffer used. The free fraction can be measured at time $t=0$. Subsequently, the total drug loading can be measured as the drug concentration at the time when equilibrium has been reached (corrected for drug degradation). Performing this experiment under different conditions also allows the investigation of drug release kinetics. Release of PTX *in vivo* occurs through the hydrolytic cleavage of the ester bond to the succinic acid moiety, with temperature and pH influencing hydrolysis in an aqueous solution. Additionally, endogenous esterases in plasma could contribute to hydrolysis. Notably, both PTX and the polymer/linker contain additional hydrolyzable bonds - four ester bonds within the PTX moiety, the amide bond attaching the succinic acid linker to the polymeric carrier, and the repeated acetal groups in the polymer (**FigureS1**). One additional consideration for drug release from a covalent bond is the potential for concomitant drug degradation. PTX is known to epimerize in an aqueous solution to 7-epi-PTX. Additional main degradation products from PTX are baccatin and 10-deacetyl-PTX.^[30,31] Although inconsistencies exist in the literature, 7-epi-PTX is assumed to possess similar bioactivity to PTX, whereas the latter two degradation products display lower bioactivity.

Table 1. Characterization of polyacetal-based conjugates

	PTX loading (wt.%)	Size (nm) ¹	PDI^2	Z^3 (mV)	Mw (kDa) ³	Mn (kDa) ³	D^4	Rh (nm) ⁵
<i>tert</i> -Ser	-	6 ± 1	0.4	1.2	27.0	15.7	1.7	5.0
<i>tert</i> -Ser-PTX	6.8	9 ± 2	0.3	1.5	23.6	34.4	1.48	6.0

¹Data obtained by DLS for 5 mg/ml solutions in PBS (mean ± SD). Size distribution by volume %; ²Polydispersity index determined by DLS; ³Z potential determined by electrophoresis light scattering in PBS ⁴Data obtained by GPC in DMF/LiBr (1%) at 8mg mL⁻¹; ⁵Radius of Hydration (Rh) determined by ¹H-diffusion ordered spectroscopy-NMR.

The initial analytical results obtained of drug loading after the spontaneous release of PTX (**Figure 1b**) suggested a possible incomplete release of PTX and/or concomitant degradation of PTX during analysis. Therefore, we devised a complementary drug quantification strategy that encompassed complete, harsh chemical degradation of both the polymer and the drug to accelerate the degradation of all hydrolyzable bonds. This strategy released two benzoic acid molecules per molecule of PTX. As no other sources of benzoic acid exist in the samples, the quantification of benzoic acid can function as a direct measure of released, degraded, and polymer-bound PTX. In the absence of biological conversion pathways (i.e., enzymes and cofactors), the chemical conversion of benzoic acid should be minimal. Moreover, the

1 conversion is known to be stable both towards strongly acidic and strongly alkaline conditions
2 that hydrolyze ester and amide bonds.
3

4 Free PTX measured as a function of incubation time in PBS with pH adjusted to 7.4, 5.5,
5 and 4.0 showed as expected, the release rate increases markedly with pH, see **Figure 1b**. The
6 initial experiments indicated a peak concentration at pH 7.4 after around 48 h at 636 ng/mL
7 followed by an almost linear decrease in concentration up to the last sampling point at 336 h,
8 suggesting PTX degradation. Sample incubation at lower pH prompted an upward trend in the
9 concentration of PTX even at the last sampling point, suggesting the incomplete release of PTX.
10 Here, the measured concentration of PTX of 592 ng/mL strongly indicates the underestimation
11 of the value measured at 48 h (pH 7.4). Upon inspection of the LC-MS/MS data, we discovered
12 a second chromatographic peak with a mass and fragmentation pattern of PTX. A comparison
13 with analytical standards allowed the identification of the 7-epi-PTX impurity. The formation of
14 this epimer seems to be accelerated at neutral and alkaline pH. Furthermore, an additional
15 control experiment carried out by incubating free PTX in the same conditions described above,
16 demonstrated loss of total PTX (the sum of PTX and 7-epi-PTX) over time, indicating the
17 degradation of both species to other molecules. This degradation could occur through the
18 hydrolysis of the ester to form baccatin.
19
20
21
22
23
24
25
26
27
28
29
30

31 **Figure 1b** shows the quantification of released PTX with 7-epi-PTX included and
32 corrected for the degradation of free PTX. After correction, the peak concentration was 1692
33 ng/mL of PTX release, which corresponds to a concentration (w/w) of 1.69 μg PTX per 25 μg *tert*-
34 *Ser*-PTX, resulting in a total PTX loading of 6.8% w/w. Using the samples at pH 4.0 and 5.5, we
35 found a free PTX level in the formulation of less than 1.5% of total drug loading. As we
36 determined a measured and calculated drug loading slightly lower than the value obtained by
37 NMR, we designed a complementary drug loading measurement strategy by inducing complete
38 chemical degradation (see **Experimental Design Considerations**) of PTX. This approach indicates
39 an absolute lower limit for drug loading, as it constitutes a direct measurement of a fragment of
40 the PTX molecule. After digestion of both free PTX and *tert*-*Ser*-PTX with 4M H_2SO_4 at 90°C
41 overnight, we measured the concentration of benzoic acid. The theoretical concentration of
42 benzoic acid in both samples was 234.2 μM . For the free PTX sample, we found a concentration
43 of 222.0 μM benzoic acid, which constitutes a 94.6% recovery of the theoretical value. For the
44 *tert*-*Ser*-PTX, we found a concentration of 161.0 μM , which constitutes 1.46 mg PTX per 25 mg
45 *tert*-*Ser*-PTX, 6% w/w. This experimental value of 73% of the value obtained by NMR constitutes
46 a lower value for PTX loading. The detailed results obtained by LC-MS/MS align well with the
47
48
49
50
51
52
53
54
55
56
57
58
59

initial results obtained by NMR; overall verification by orthogonal measurements techniques provides additional confidence.

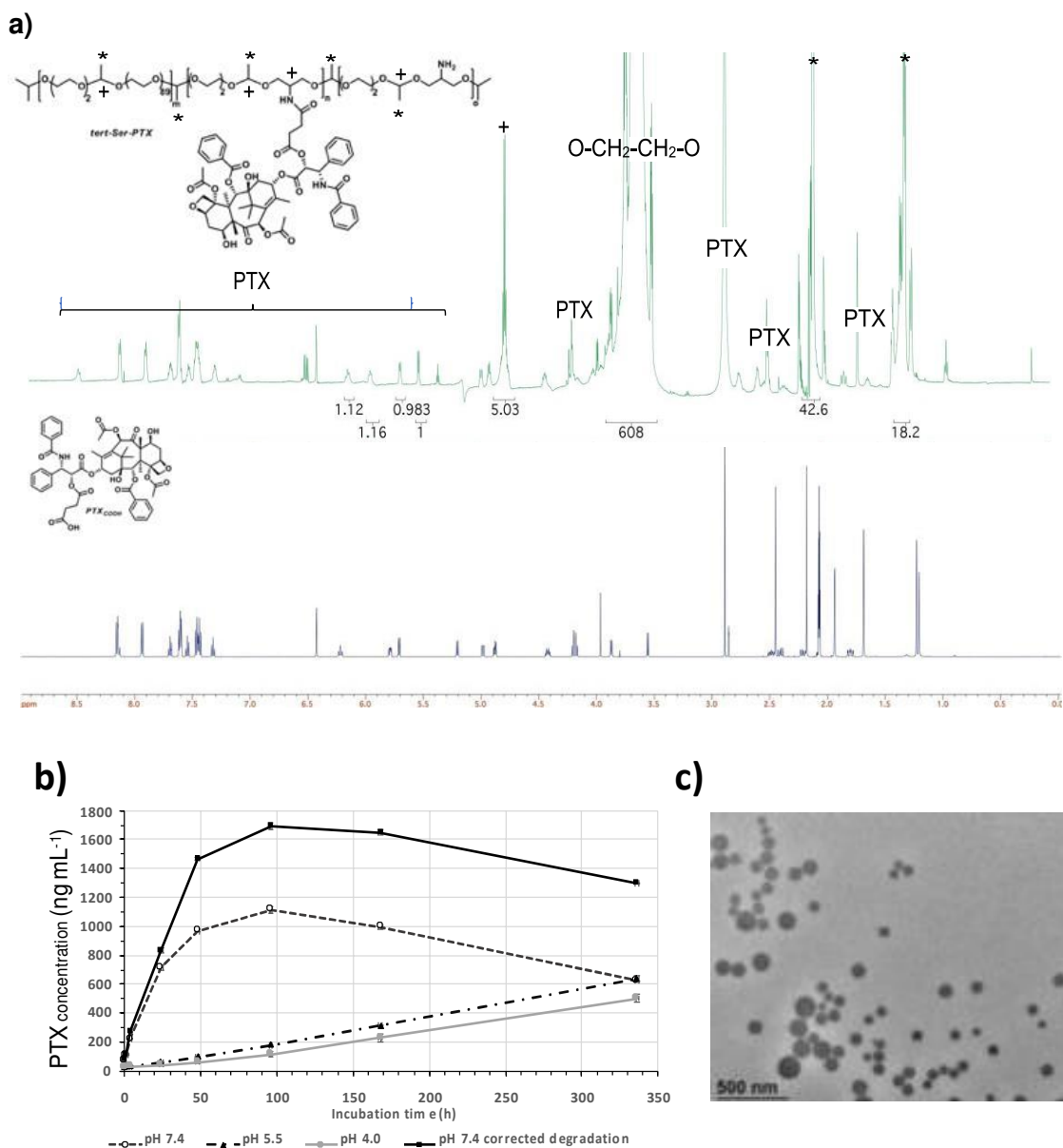


Figure 1. Characterization of *tert*-Ser-PTX **a)** High resolution 600 MHz ^1H NMR spectrum of *tert*-Ser-PTX (upper) with assigned signals and comparison with free PTX (lower). **b)** Cumulative PTX release from *tert*-Ser-PTX after incubation in PBS at 4 varying pH values (see legend) measured by LC-MS/MS. Graph shows total PTX release, including 7-*epi*-PTX epimer, without correction for PTX degradation (direct measurement for pHs 7.4, 5.5, and 4.0), and the concentration of total PTX at pH 7.4 with correction for degradation of free PTX (solid black line) as measured in a separate sample. Data as mean \pm SD ($n \geq 3$). **c)** Representative image of *tert*-Ser-PTX show a smaller and more abundant population at around 10 nm, medium-sized particles ranging from 30 to 70 nm, and a few aggregates of 200 nm.

1 DLS, diffusion ¹H-diffusion ordered spectroscopy (DOSY)-NMR (Figure S2-S3a), and SEC
2 analyses of *tert*-Ser-PTX combined to establish an average size distribution of around 9-12 nm
3 (data expressed in volume) with the presence of a small percentage of larger aggregates as
4 expected for neutral conjugates (Z potential = 1.5 mV) with hydrophobic moieties (Table 1). Of
5
6 note, we observed *tert*-Ser-PTX stability for up to 24 h in PBS, with size not significantly affected
7
8 during the incubation time (Figure S3b). Importantly, Transmission Electronic Microscopy (TEM)
9
10 analysis also demonstrated the well-dispersed nature of the particles after preparation in dry
11
12 conditions, but we observed particles of at least three families of size: the most prevalent of
13
14 small particles around 10-15 nm, medium particles of 30 to 70 nm, and a few larger particles of
15
16 around 200 nm (Figure 1d, Figure S3c).

17
18 We also investigated *tert*-Ser-PTX by SANS (methodology and data analysis are detailed in
19
20 the Supporting Information). SANS provides detail regarding the size and morphology of
21
22 structures in solution and can link different aspects of conjugate behavior to morphology. We
23
24 studied *tert*-Ser-PTX in deuterated methanol solution (MeOD) and PBS (dPBS) at 10 mg/mL
25
26 concentration, which allows the evaluation of the specific influence of PTX solvophobicity
27
28 (significantly increased in PBS compared to methanol solution). Data revealed two regions in the
29
30 scattering; at low Q, a steeper decline in I(Q) vs. Q was followed at intermediate and high Q by
31
32 a shallower and non-linear Q dependence (Figure 2).

33
34 In methanol, low Q data showed a Q⁻¹ dependence at low Q and were fitted in FISH
35
36 software. Data at low Q and intermediate/higher Q were fitted separately to a model for rods.
37
38 The parameters were then refined using the whole data set to give a combined model for two
39
40 sets of rods in solution, which was previously used for conjugates of this type.^[13] The high Q
41
42 region indicated short, thin rods with a radius of 0.7 ± 0.05 nm and a length of 17.0 ± 1.00 nm.
43
44 We also observed larger, more globular structures with a radius of 78.0 ± 2.00 nm and a length
45
46 of 50.0 ± 2.00 nm co-existing in solution.

47
48 In PBS solution, we observed a much higher intensity at low Q, which indicates larger
49
50 structures present in solution at an equivalent concentration of the same material. The high Q
51
52 data suggested the presence of broader rods in PBS compared to methanol. We also identified
53
54 a fitted radius of 1.0 ± 0.05 nm (with the fitting insensitive to rod length), suggesting the
55
56 existence of long thin structures indicative of fiber-like structures. Combined with the larger
57
58 radius in PBS compared to methanol, the presence of PTX may drive polymer chain aggregation.
59
Furthermore, considering the solvent contributions, the drug interactions would be much
weaker in an ionic solvent.

As we could not fit the whole of the PBS data to a model for two separate populations of rods. Instead, we adopted a broad peak model, typically used for large structures caused by the aggregation of other rod-like structures (e.g., fiber bundles). This model provides information on the packing of structures within the aggregate, given by the scattering at low Q , and information on the individual chains within the aggregate, given by scattering at intermediate and high Q .

When low Q Porod scattering dominates, and the slope of the straight line (n) arises from scattering from either a mass ($n = 1 - 3$) or surface ($n = 3 - 4$) fractal. Indicative values are 1 for long rigid structures, 2 for Gaussian chains, and 3 for collapsed polymer systems. The individual chains within the aggregate are characterized by a correlation length ξ , peak position Q_0 , and the fractal dimension m . The relation of these terms to $I(Q)$ is given in **Equation 1** below, where two scaling factors determine the contributions of each term.^[32] For the *tert*-Ser-PTX sample in PBS, the fitted parameters are in **Table S2**.

$$I(Q) = \frac{I_P(0)}{Q^n} + \frac{I_L(0)}{1 + (|Q - Q_0|\xi)^m} + bkg \quad \text{Equation 1.}$$

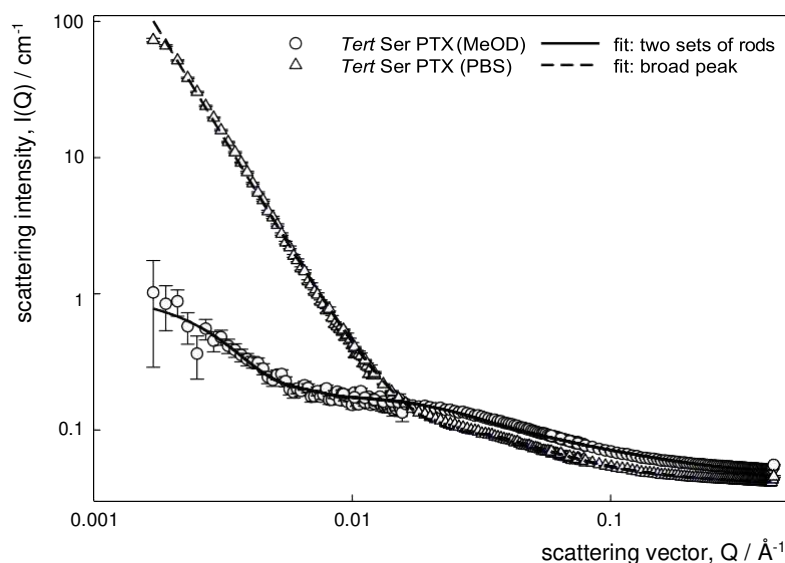


Figure 2. Characterization of *tert*-Ser-PTX by SANS. SANS data from 1 wt.% conjugate solutions in dPBS and MeOD. Representative error bars are shown.

To summarize, we found *tert*-Ser-PTX scattering patterns consistent with the formation of large globular structures of ~ 100 nm in diameter co-existing with long thin rod-like structures in methanol; however, we observed more ordered structures in PBS (**Figure 2**). The modeling

1 results suggest the aggregation of rods into densely packed bundles in PBS. The rods themselves
2 in PBS are thicker (about 1.5 x) than in methanol, consistent with the intramolecular association
3 of PTX molecules, which increases the stiffness of the rod-like structures and drives
4 intramolecular alignments into bundles (**Figure 2** and **Table S2**). Notably, the smaller structures
5 observed by SANS are consistent with the sizes obtained from DLS. These findings could suggest
6 that sample filtration before DLS measurements remove or disrupt any larger structures
7 present, which leaves insufficient time for reformation. The scattering results from the *tert*-Ser-
8 PTX sample fit best to a thin rod of radius 10 Å, length 300 Å, with a Q^{-n} term with $n=3.5$ (**Figure**
9 **2** and **Table S2**).

10 11 12 13 14 15 16 17 18 **2. *tert*-Ser-PTX stability and drug release studies in simple and complex media**

19
20
21 Stability during circulation and the potential for controlled drug release from the polymeric
22 carrier under selected physiological triggers represent two essential characteristics of PDCs.^[13]
23 While the released free drug fraction supports biological outcomes, the (reversibly) released
24 fraction bound to plasma or cell medium proteins constitutes a 'reservoir' in equilibrium with
25 free PTX. Therefore, we must understand the levels of both free and total released PTX.
26
27

28
29 In the absence of serum, the percentage release of PTX from *tert*-Ser-PTX displayed a pH-
30 dependent profile, with an increase in PTX release upon increased pH (**Figure 3a**). We note that
31 this is an unexpected result for polyacetal systems^[11-13], which generally degrade (and therefore
32 release the conjugated active agent) more rapidly at a lower, acidic pH. Our previous studies
33 involved incorporating drugs directly into the polymer backbone; however, the conjugate
34 described in this study employs a polymer-drug linker susceptible to hydrolysis. This provides
35 two possible mechanisms of PTX release from the polyacetal polymer involving hydrolysis: i)
36 hydrolysis of acid pH-sensitive polymer backbone acetal bonds or ii) hydrolysis of the ester
37 bonds of the polymer-drug linker (**Figure S1**). Overall, our results suggest drug release driven by
38 hydrolysis of the polymer-drug linker. PTX release at pH 7.4 is hydrolytically triggered by ester
39 bond degradation; in buffer, this degradation is faster than the disruption of the polyacetal
40 main chain at pH 5.5, as we observed no significant metabolites containing Ser-PTX moieties
41 (data not shown).
42
43
44
45
46
47
48
49
50
51
52
53
54
55
56
57
58
59

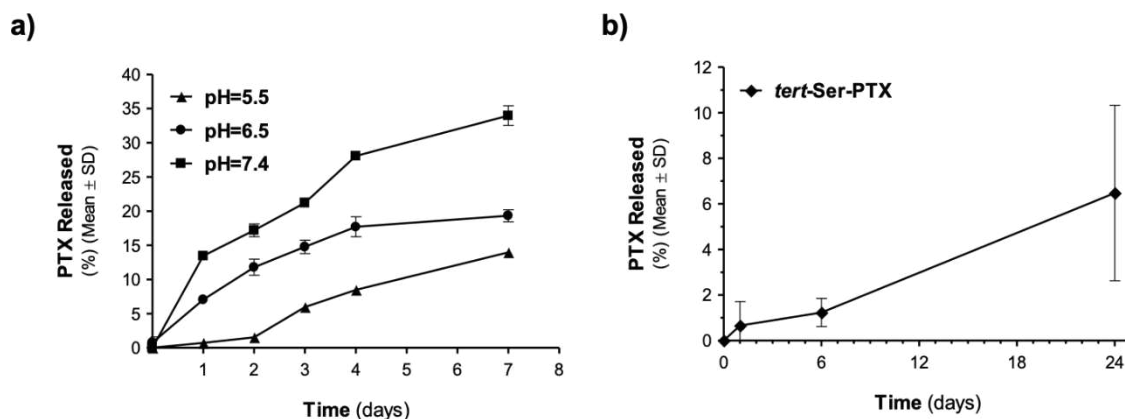


Figure 3. PTX release from *tert*-Ser-PTX in PBS and rat serum. a) pH-dependent release (3 mg mL^{-1} , 37°C) in PBS at pH 5.5, 6.5, and 7.4 determined by HPLC-UV. **b)** Effect of rat serum on release (3 mg mL^{-1} , 37°C). Data as mean \pm SD ($n \geq 3$).

In the presence of rat serum, *tert*-Ser-PTX released low levels of PTX during a 24 h incubation at pH 7.4 (**Figure 3b**). Therefore, our data suggest that serum proteins protect the ester bond from hydrolytic degradation; however, the role of *in vivo* protein corona formation^[33] in the protection of the *tert*-Ser-PTX ester bond requires further consideration. In any case, this is an encouraging finding as increased stability in serum favors systemic administration.^[34] Overall, we found less than 2% of total PTX release after 6 h incubation at 37°C , and less than 7% after 24 h incubation.

We performed further exhaustive analyses using LC-MS/MS to ratify our hypothesis - although we employed three different concentrations (see **Materials and Methods**). The data provided similar trends; thus, we here present only the $2 \mu\text{g mL}^{-1}$ concentration point (the most clinically relevant concentration) in the following discussion for clarity (**Figure 4** and **Figure S4**).

Figure 4a-b demonstrates evident differences in release and/or degradation kinetics in different media (in both panels, 'sPTX' denotes the sum of PTX and 7-epi-PTX). We found low or negligible variability between replicates at most data points. Of note, we buffered the pH in PBS, RPMI, and plasma to 7.4, although HepG2 medium remained unbuffered (manual evaluation of several samples of HepG2 medium indicated a pH of around 8.0). In comparison with our drug loading studies, we observed the accelerated release of sPTX at higher pH (and we presumed this to cause the accelerated release of sPTX in HepG2 medium compared to RPMI and plasma). Furthermore, the increased degradation of sPTX in HepG2 medium may correlate to the increased susceptibility of the intramolecular ester bond to hydrolysis at elevated pH.

Of note, the measured concentrations of released sPTX in PBS, RPMI, and plasma

1 converge on equilibrium values, albeit at distinct levels; for plasma, the concentration converges
2 towards the theoretical loading of 2,000 ng/mL after two weeks. We observed a similar initial
3 shape for the sPTX release curves for PBS, RPMI, and plasma; however, the subsequent plateau
4 for each condition occurs at distinct concentrations. We also note that similar total protein levels
5 present in HepG2 and RPMI media (10% FBS in HepG2; 10% plasma in RPMI) remain much lower
6 than that found in total human plasma. Therefore, one could speculate that the differences at
7 later time points may correlate with solubility limits in the respective media, as observed by
8 Abouelmagd et al.^[35]
9

10
11
12
13
14
15 As PTX suffers from an extremely high degree of protein binding, the increased amount
16 of protein in media (RPMI, plasma) may ensure an increased amount of solubilized sPTX.
17 Interestingly, PTX release into plasma extends beyond two weeks with little or no loss of sPTX
18 observed during this time, even as measured concentrations approach theoretical PTX loading.
19 This may indicate that plasma proteins contribute to PTX stabilization and protection of PTX
20 from degradation, thereby corroborating our hypothesis. Degradation may occur in PBS in a
21 comparable manner to our observations in drug loading experiments (**Figure 1b**); however, this
22 remains undetectable, as precipitated PTX would re-solubilize concomitantly up to the solubility
23 limit. The complete evaluation of this hypothesis would require longer incubation times or the
24 direct detection of degradation products.
25
26
27
28
29
30
31
32

33
34
35
36
37
38
39
40
41
42
43
44
45
46
47
48
49
50
51
52
53
54
55
56
57
58
59
60
61
62
63
64
65

Figure 4b depicts the conversion of PTX to 7-epi-PTX, which occurs to a significant degree in all media and reaches near completion in HepG2 medium. For PBS and RPMI, the conversion kinetics remain similar to those for plasma. These findings strongly advise the detailed investigation of the biological effect equivalence between PTX and 7-epi-PTX, as the latter compound could be the predominant epimer in plasma after around three days. **Figures 4c and S4a** show the corresponding levels of free drug (sPTX) measured after spin filtration (i.e., excluding protein-bound drug) in the respective media. While the equilibrium concentrations measured in the supernatant from the PBS, RPMI, and plasma remain comparable after two weeks. Analysis in HepG2 medium revealed little detectable sPTX at longer incubation times, reinforcing the hypothesis that PTX degrades more rapidly in this medium. Even given the relatively large degree of variability for the HepG2 samples (and PBS) at 24 h, the notably high sPTX concentration found in the centrifuged supernatant could indicate that either pH or other compounds present in HepG2 medium effectively increase the aqueous solubility of PTX. We also note the low variability between replicates at the other sampling points.

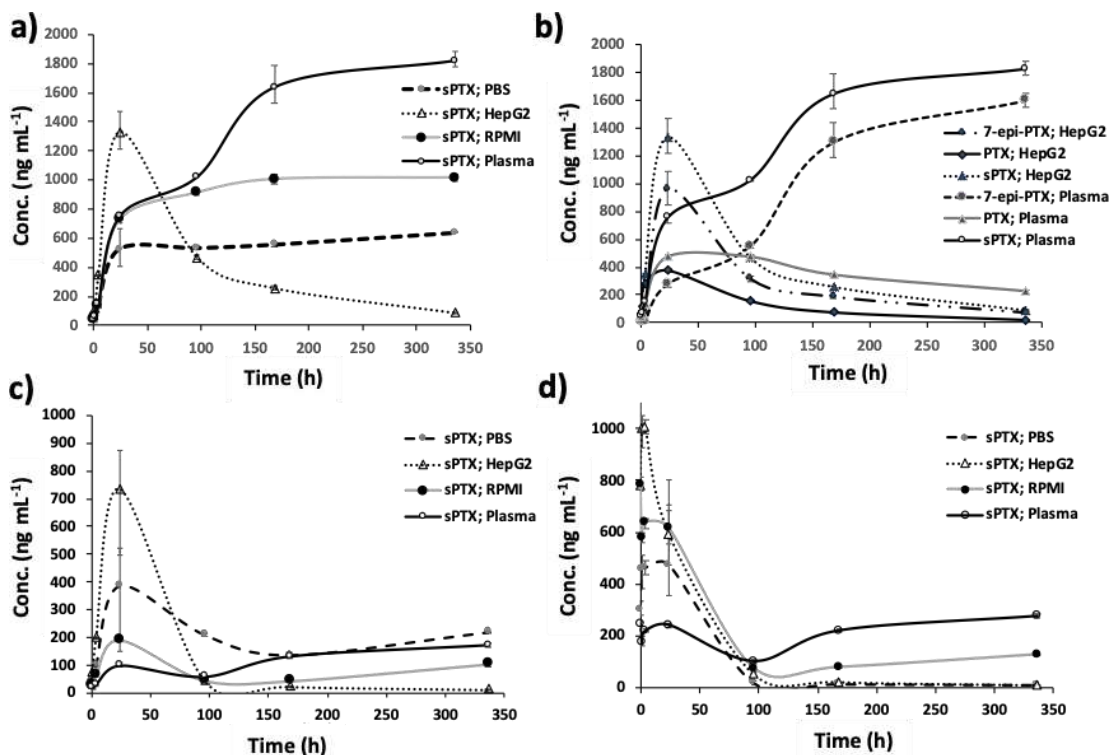


Figure 4. **a)** PTX released from *tert*-Ser-PTX after incubation in different media (PBS, RPMI cell medium, HepG2 cell medium, human plasma), measured by LC-MS/MS as the sum (sPTX) of PTX and 7-epi-PTX. **b)** Release into HepG2 cell medium and human plasma plotted as the single components PTX and 7-epi-PTX and the sum. RPMI and PBS showed similar ratio trends between PTX and 7-epi-PTX as human plasma but were omitted for visual clarity. **c)** PTX released from *tert*-Ser-PTX after incubation in different media (PBS, RPMI cell medium, HepG2 cell medium, human plasma), measured by LC-MS/MS as the sum (sPTX) of PTX and 7-epi-PTX, after centrifugal ultrafiltration (i.e., excluding protein-bound drug). **d)** Free PTX after incubation in different media (PBS, RPMI cell medium, HepG2 cell medium, human plasma), measured by LC-MS/MS as the sum (sPTX) of PTX and 7-epi-PTX, after centrifugal ultrafiltration (i.e., excluding protein-bound drug). Data as mean \pm SD ($n \geq 3$).

Finally, a comparison, with the same amount of free PTX added as control, for the free drug after ultrafiltration is presented in **Figures 4d** and **S4Sb**. We added free PTX solubilized in an organic solvent (acetonitrile); while this was necessary given the solubility profile of PTX, we appreciate that this could induce local precipitation effects and other potential inhomogeneities. Nevertheless, the availability of free sPTX after long incubation times correlates with the amount of protein in the medium, which conceivably acts as a depot to protect PTX from degradation, as demonstrated in **Figures 4d** and **S4b**. The loss of free PTX over time compared to *tert*-Ser-PTX is of interest (we detected free PTX during the whole incubation period), which may derive from continuous release from the conjugate. The almost complete

1
2
3
4
5
6
7
8
9
10
11
12
13
14
15
16
17
18
19
20
21
22
23
24
25
26
27
28
29
30
31
32
33
34
35
36
37
38
39
40
41
42
43
44
45
46
47
48
49
50
51
52
53
54
55
56
57
58
59
60
61
62
63
64
65

loss of free sPTX over time for the HepG2 medium corresponds well with our observations regarding *tert*-Ser-PTX incubation, i.e., loss most likely reflects elevated levels of degradation.

In summary, *tert*-Ser-PTX conjugate provides for the sustained release of PTX over two weeks, which reaches the theoretical limit regarding PTX loading. PTX release markedly accelerates at alkaline pH (or in the presence of specific degradation factors in the HepG2 cell medium), as does PTX degradation. Furthermore, the significant degree of epimerization of PTX to 7-epi-PTX must be considered for any assessment of bioactivity.

3. *In vitro* efficacy of *tert*-Ser-PTX

To further explore drug-release and efficacy, we incubated androgen-dependent and androgen-independent PCa cell lines with increasing concentrations of *tert*-Ser-PTX and compared results to free PTX. Free PTX and *tert*-Ser-PTX treatment reduced cell viability in both cell lines, and *tert*-Ser-PTX displayed a higher IC₅₀ value than free PTX (**Figure 5** and **Table 2**). We obtained lower IC₅₀ values for *tert*-Ser-PTX in LNCaP cells ($0.152 \pm 0.141 \mu\text{g PTX mL}^{-1}$) compared to PC-3 cells ($0.764 \pm 0.381 \mu\text{g PTX mL}^{-1}$) (**Table 2**), suggesting the increased sensitivity of the androgen-dependent LNCaP cells.

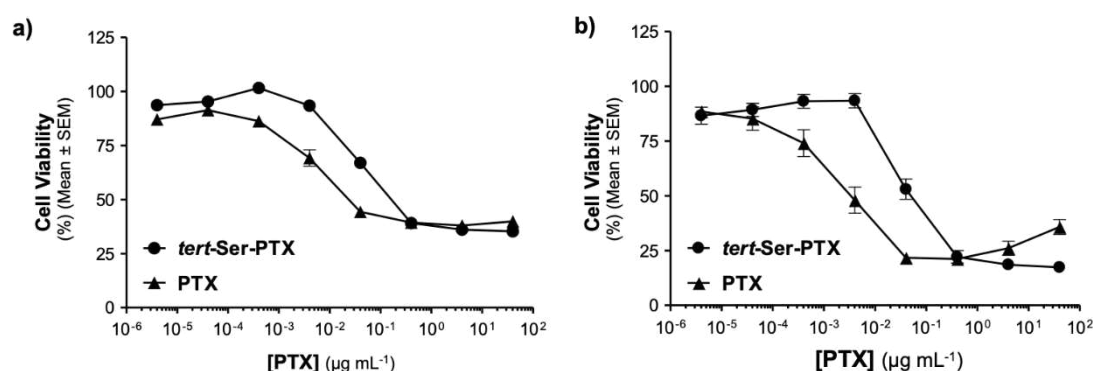


Figure 5. *In vitro* efficacy of *tert*-Ser-PTX in PCa cell lines. MTT assays were performed after 72 h incubation of **a)** androgen-independent PC-3 and **b)** androgen-dependent LNCaP PCa cells with increasing concentrations of *tert*-Ser-PTX or free PTX.

Interestingly, we found the greater efficacy of *tert*-Ser-PTX at high concentrations of PTX (>0.4 μg mL⁻¹) when compared to the free drug in both cell lines, but especially in LNCaP cells (**Figure 5c**). We previously observed that free PTX does not entirely abolish cell viability and that increasing the drug concentration does not result in higher cytotoxic activity in colon and breast cancer cell lines.^[36] This result could be driven by the existence of PTX drug resistance

mechanisms such as the presence of P-glycoprotein 1 (P-gp) (also known as multidrug resistance protein 1 (MDR1) or ATP-binding cassette sub-family B member 1 (ABCB1)), which pumps the cytotoxic drug out of the cell.^[19,37] Therefore, applying a drug delivery system that introduces drugs through the endocytic pathway might overcome this problem.^[38]

Table 2. IC₅₀ values for free PTX and *tert*-Ser-PTX in different PCa cells. Each value is mean ± SEM (*n* = 3).

PCa cell line	IC ₅₀ (µg PTX mL ⁻¹)	
	PTX	<i>tert</i> -Ser-PTX
PC-3	0.067 ± 0.027	0.764 ± 0.381
LNCaP	0.007 ± 0.003	0.152 ± 0.141

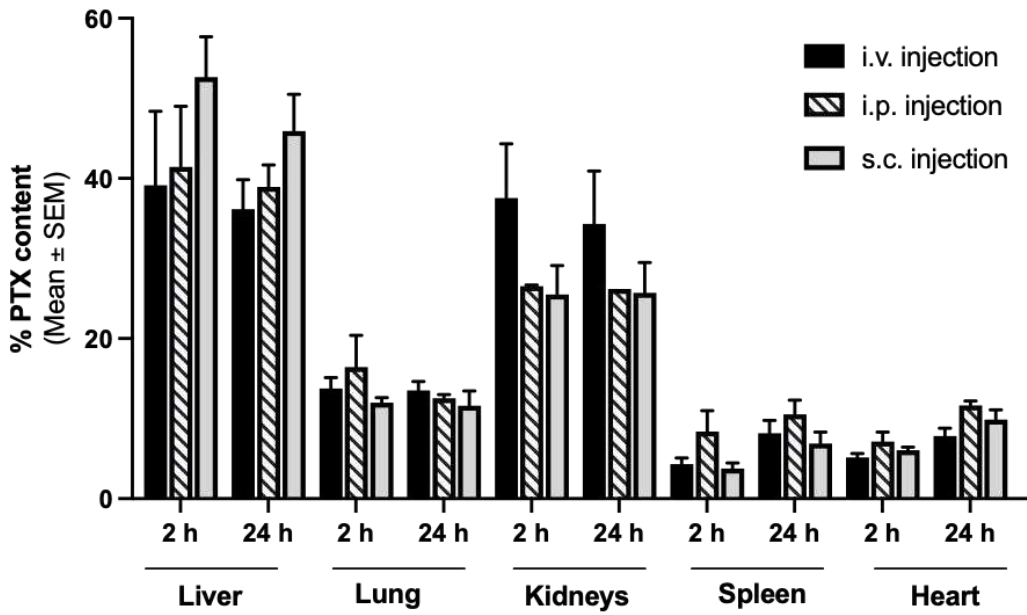
4. *In vivo* biodistribution of *tert*-Ser-PTX

Next, we evaluated the biodistribution of *tert*-Ser-PTX as results of different routes of administrations (**Figure 6a**). This was carried out before the efficacy assessment.

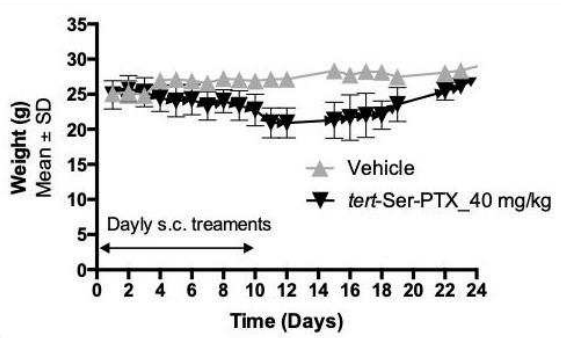
The results indicate that most of the administered PTX located to the liver (36.1 ± 4.5% for i.v. injection at 24 h) and kidneys (34.3 ± 8.1% for i.v. injection at 24 h), regardless of the injection route. From the safety toxicity perspective, we observed no significant differences between the different administration routes. While PTX is i.v. administered in the clinical setting, we performed daily s.c. administrations of *tert*-Ser-PTX at high doses (40 mg kg⁻¹, 10 doses) during the r-MTD safety study. This was done with the intention of improving the consistency while reducing animal stress. Weight monitoring of the animals showed that repeated *tert*-Ser-PTX administrations induced mild weight loss in both sexes during the treatment period, which was fully recovered during the 14 days of follow-up. **Figure 6b**, shows weights of male mice, sex where we observed the most significant differences between vehicle to *tert*-Ser-PTX treated mice). We also did not observe any behavioral changes during the treatment or observation periods. **Histological assessment of different organs in these animals post treatment did not detect any abnormalities in lung, kidney, spleen, and heart; only in liver tissue mitotic changes were detected, probably due to the high concentration of PTX. These results showed that *tert*-Ser-PTX was safe to use for repeated administrations up to a maximum dose of 40 mg kg⁻¹ in PTX load. Upon the presence of moderate changes in liver histology, a lower PTX doses was adopted (15 mg kg⁻¹ in PTX) for tolerability studies, as described next.**

1
2
3
4
5
6
7
8
9
10
11
12
13
14
15
16
17
18
19
20
21
22
23
24
25
26
27
28
29
30
31
32
33
34
35
36
37
38
39
40
41
42
43
44
45
46
47
48
49
50
51
52
53
54
55
56
57
58
59
60
61
62
63
64
65

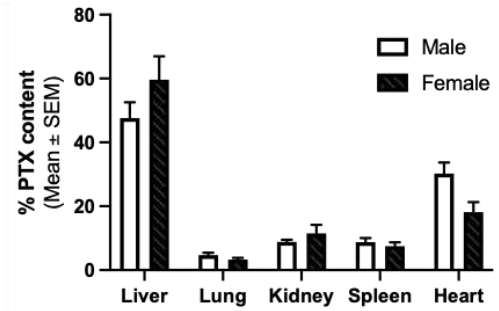
a)



b)



c)



d)

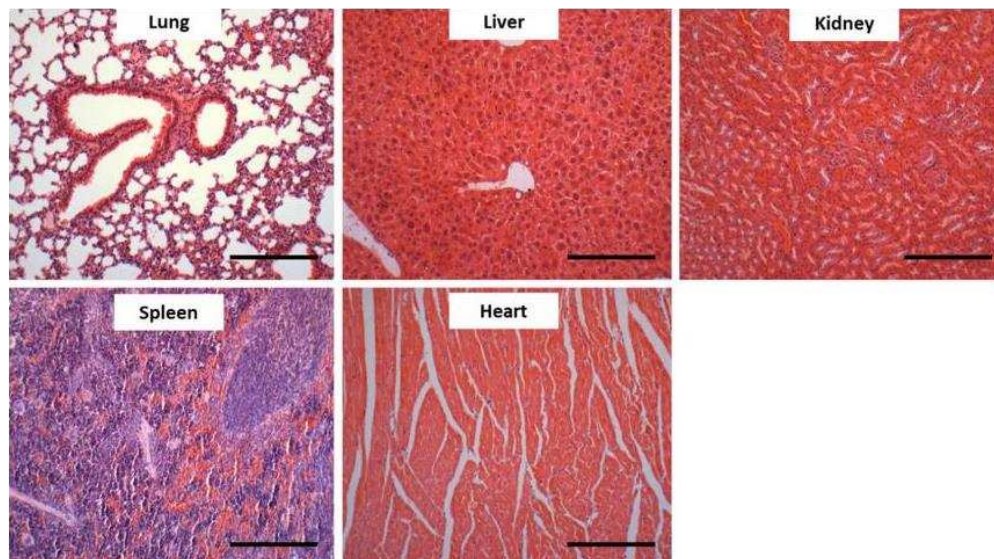


Figure 6. *In vivo* biodistribution and safety after single-dose and repeated administration of *tert*-Ser-PTX. C57BL/6 mice were administered with a single dose at 20 mg kg⁻¹ or repeated administrations of 40 mg kg⁻¹ *tert*-Ser-PTX at PTX-equivalent doses. Thereafter, PTX content was determined by LC-MS/MS analysis. **a)** PTX biodistribution among different organs 2 and 24 h after single i.v., i.p., or s.c. injection (*n*=2-3 per time point). **b)** Weight monitoring in male animals receiving 10 s.c. doses of 40 mg kg⁻¹ *tert*-Ser-PTX (*n*= 4). **c)** PTX content in organs of male and female mice after ten s.c. administrations of 40 mg kg⁻¹ *tert*-Ser-PTX (*n*=8, 4 males and 4 females). **d)** representative histological H&E images of lung, liver, kidney, spleen and heart tissue slices collected from a representative male mouse treated with 10 doses of 40 mg kg⁻¹ *tert*-Ser-PTX (Scale bar = 250 μm).

5. *In vivo* PTX tolerability of *tert*-Ser-PTX

We treated mice bearing orthotopic LNCaP.Fluc2 tumors with free PTX and *tert*-Ser-PTX and investigated toxicity by monitoring body weight and physical and clinical observations.

Table 3. Main parameters monitored in toxicity evaluation of PTX and *tert*-Ser-PTX after repeated administration of 15 mg kg⁻¹ of PTX equivalents.

	PTX Vehicle	PTX	<i>tert</i> -Ser-PTX Vehicle	<i>tert</i> -Ser-PTX
Found dead or euthanized due to side effects	0/9 (0%)	9/9 (100%)	0/9 (0%)	0/9 (0%)
Enlarged urinary bladder	0/9 (0%)	7/9 (78%)	0/9 (0%)	0/9 (0%)
Enlarged kidneys	0/9 (0%)	2/9 (22%)	0/9 (0%)	0/9 (0%)

The toxicity of PTX and *tert*-Ser-PTX and their respective vehicles (Ethanol:Cremophor EL:Saline for PTX and PBS for *tert*-Ser-PTX). The number of animals and the corresponding percentage (in brackets) are given.

As summary of the data from the animal welfare monitoring is provided for this study in **Table 3**. Of note, two animals from the group treated with free PTX died 24 h after treatment, while the remaining animals displayed signs of toxicity and were euthanized a week after treatment initiation. After necropsy, we observed macroscopic lesions such as an enlarged urinary bladder (7/9 (78%)) and clear and enlarged kidneys (2/9 (22%)); however, we failed to observe similar lesions in the *tert*-Ser-PTX treated group (**Table 3**). Additionally, we failed to encounter significantly adverse effects on animal body weight, although we did detect fur alteration and black faces as minor adverse side effects after the first week of administration. By the end of the treatment period, we observed a treated to control (T/C) ratio of body weight change of -3% for the *tert*-Ser-PTX treated animals. Notably, the toxicities observed for free PTX

1 at specific concentrations became significantly reduced following polymer conjugation (treating
2 with the same concentration of PTX equivalents). Blood samples showed no differences in
3 biochemical parameters between the *tert*-Ser-PTX and vehicle-treated mice (Table S3),
4 indicating the safety of repeated administrations of *tert*-Ser-PTX in animals. Overall, we found
5 that *tert*-Ser-PTX was well tolerated and failed to cause adverse effects or animal deaths over
6 the treatment period.
7
8
9

10
11 Our results indicate that polyacetals might constitute a promising drug delivery system
12 that reduces systemic PTX toxicity by avoiding Cremophor and improvements to tissue
13 biodistribution, as demonstrated for other PTX delivery systems.^[39] Currently, two clinically
14 approved nanoparticle taxane (i.e., PTX family of compounds) formulations exist - nab-PTX
15 (Abraxane™, Abraxis Bioscience, Los Angeles, USA) and Genexol-PM (Samyang Biopharm,
16 Daejeon, South Korea). While both formulations increase the maximum tolerated dose of
17 PTX,^[40] dose-limiting toxicities such as neutropenia, myalgia, and neuropathy remain significant
18 problems, and improvements to clinical outcomes remain modest^[39,40]. Therefore, we still
19 require further development/refinements of drug delivery systems to improve efficacy and
20 safety profiles, including a direct comparison of *tert*-Ser-PTX polymers with already approved
21 PTX formulations.
22
23
24
25
26
27
28
29
30
31
32
33

34 6. Inhibition of orthotopic tumor growth by *tert*-Ser-PTX

35 We next orthotopically implanted LNCaP.Fluc2 cells into the mouse prostate and non-
36 invasively monitored tumor growth through bioluminescent optical imaging to determine the
37 anti-tumor efficacy of *tert*-Ser-PTX. We treated *tert*-Ser-PTX and free PTX (group ended a week
38 after treatment initiation, as indicated above) groups via i.v. injection with the maximum
39 tolerated dose of free PTX (15 mg kg⁻¹ PTX-equivalent dose) three times a week every second
40 week for four weeks. We quantified the growth rate of primary tumors from the ventral
41 abdominal region over time via bioluminescent intensity as the intra-abdominal location of the
42 tumor precluded direct measurement of tumor volume. Figure 7 demonstrates the
43 bioluminescent signal in the vehicle control and *tert*-Ser-PTX treated-group over time. The BLI
44 intensity measurements and direct images demonstrated that LNCaP.Fluc2 tumors treated with
45 the *tert*-Ser-PTX conjugate at 15 mg PTX kg⁻¹ did not significantly change in size compared to the
46 vehicle control group, which displayed an exponential increase of bioluminescent signal within
47 the prostate (Figure 7a). These differences were reflected when calculating bioluminescent
48 absolute growth delay, relative tumor bioluminescence, and T/C ratio.
49
50
51
52
53
54
55
56
57
58
59

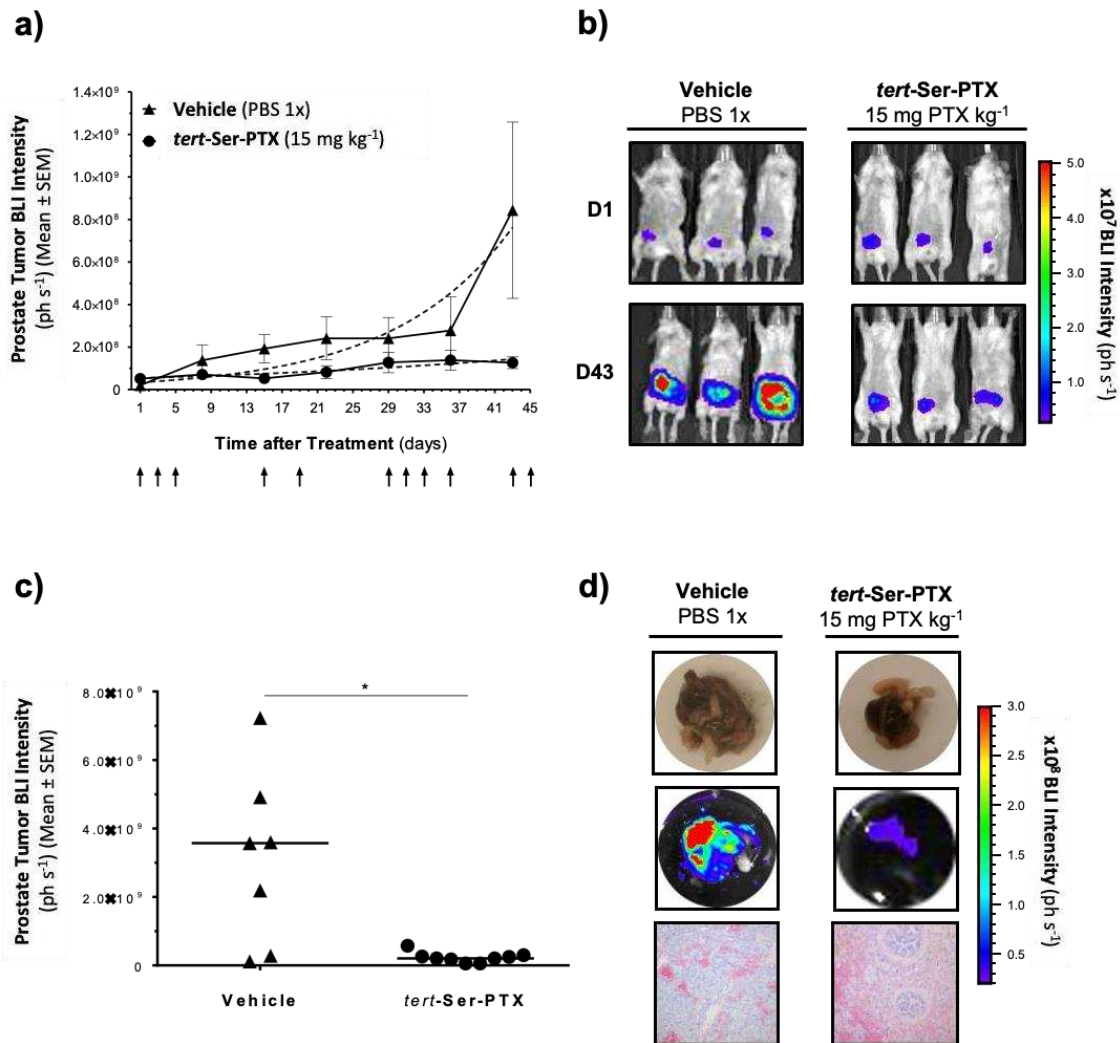


Figure 7. In vivo impact of tert-Ser-PTX treatment on orthotopic LNCaP.Fluc2 tumor growth. Comparative analysis of PCa growth longitudinally and at the endpoint following treatment with tert-Ser-PTX i.v. administered at 15 mg PTX kg⁻¹ or vehicle as a control. **a)** Primary tumor growth rate from the ventral abdominal region was quantified weekly using bioluminescent intensity (ph s⁻¹). The dotted line indicates the non-linear regression fits of exponential tumor growth. Arrows on the X-axis indicate the administration schedule. **b)** Representative examples of mouse bioluminescence (ventral views) from tert-Ser-PTX and vehicle control groups are shown over the treatment timeline. **c)** Scatter dot plots of prostate tumor bioluminescence ex vivo at day 46 (study endpoint). **d)** Ex vivo comparisons of gross morphology, bioluminescence, and histopathology of LNCaP.Fluc2 tumors treated with vehicle or 15 mg kg⁻¹ of tert-Ser-PTX. The mean or median BLI intensities and corresponding standard errors of the mean (SEM) were determined and plotted (n ≥ 7). The significance threshold was established at p < 0.05, and significance levels were schematically assigned * (0.01 ≤ p < 0.05), ** (0.001 ≤ p < 0.01), *** (0.0001 ≤ p < 0.001) or **** (p < 0.0001).

1 On day 43 (day 46 represents the endpoint of the study) of treatment, we found a delay in
2 bioluminescent absolute growth delay of 21 days for the *tert*-Ser-PTX treated group, and relative
3 tumor bioluminescence values of 1821% and 481% for vehicle and *tert*-Ser-PTX, respectively,
4 demonstrating the smaller nature of the tumors (and the lower levels of emitted
5 bioluminescence) from *tert*-Ser-PTX treated mice. Finally, we found a T/C ratio of tumor
6 bioluminescence of 26% for *tert*-Ser-PTX, indicating the robust inhibition of tumor growth in
7 those animals treated with the *tert*-Ser-PTX.
8
9

10
11
12
13 At the endpoint of the experiment (day 46), *ex vivo* tumor bioluminescence and *ex vivo*
14 tumor weight analyses further confirmed statistically significant tumor growth inhibition (**Figure**
15 **7c** - $p=0.0164$ and Figure S2, $p=0.0464$, respectively). We also found T/C ratios for tumor weight
16 and tumor bioluminescent growth of 17% and 8%, respectively, for the *tert*-Ser-PTX treated
17 group.
18
19

20
21 Thus, *tert*-Ser-PTX at 15 mg PTX kg⁻¹ administered at the above-noted schedule significantly
22 inhibited tumor growth compared to the vehicle control group. Moreover, *ex vivo* analysis of
23 prostates and histological images (**Figure 7c**) revealed that cancer cells occupied the whole
24 prostatic gland in the vehicle control group, while *tert*-Ser-PTX treated mice displayed typical
25 prostate structures and the maintenance of gland histology. Overall, these findings confirm the
26 elevated antitumoral efficacy of PTX formulated as a polyacetal-based polymer therapeutic.
27
28
29

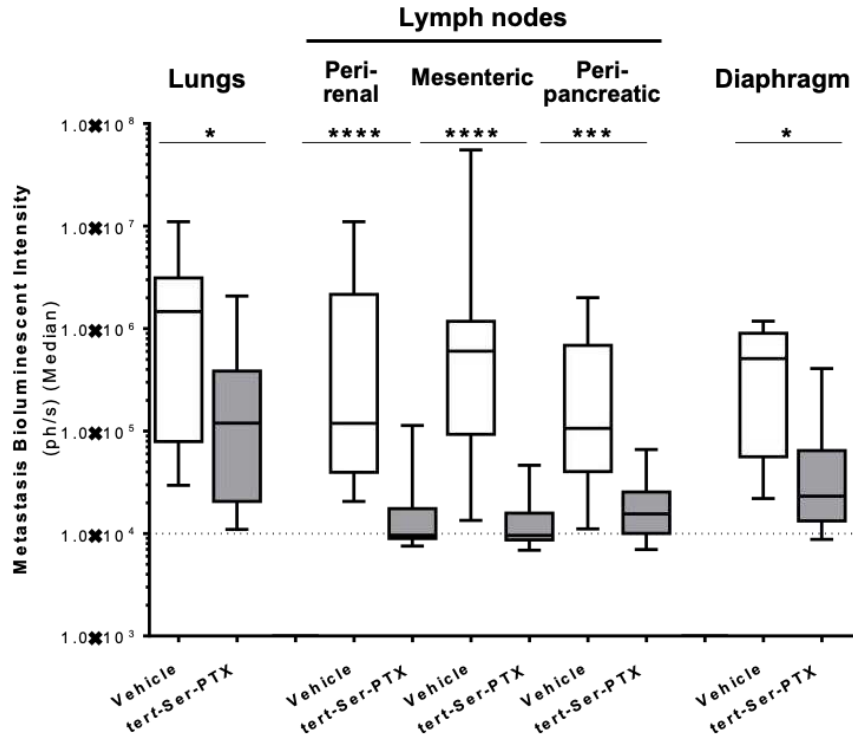
30
31 We also note that the obtained results improve on those found for the i.v. administration
32 of a novel anti-microtubule agent (LG308),^[41] an albumin-binding prodrug of PTX,^[42] PTX
33 microspheres,^[43] and PEG-based PTX -polymers^[44] in orthotopic PCa models.
34
35
36
37
38
39
40
41

42 **7. Inhibition of distant and locoregional metastasis by *tert*-Ser-PTX**

43

44 The orthotopic implantation of tumor cells into the prostate provides a PCa model that
45 includes all steps of metastatic progression that resembles the human clinical setting.^[45] The
46 LNCaP.Fluc2 orthotopic PCa model employed mimics the clinical pattern of spontaneous PCa
47 metastases, including lymphatic, hematologic, and coelomic dissemination. At the experimental
48 endpoint, *ex vivo* BLI and histopathological evaluation of excised tissues allowed the
49 identification and localization of sites of spontaneous metastases (incidence rates) for *tert*-Ser-
50 PTX and vehicle control-treated groups (see **Supplementary Information Table S4**). Significantly,
51 *tert*-Ser-PTX reduced the incidence of metastases from orthotopic prostate LNCaP.Fluc2 tumors
52 when administered at a concentration of 15 mg PTX kg⁻¹ at the described schedule.
53
54
55
56
57
58

a)



b)

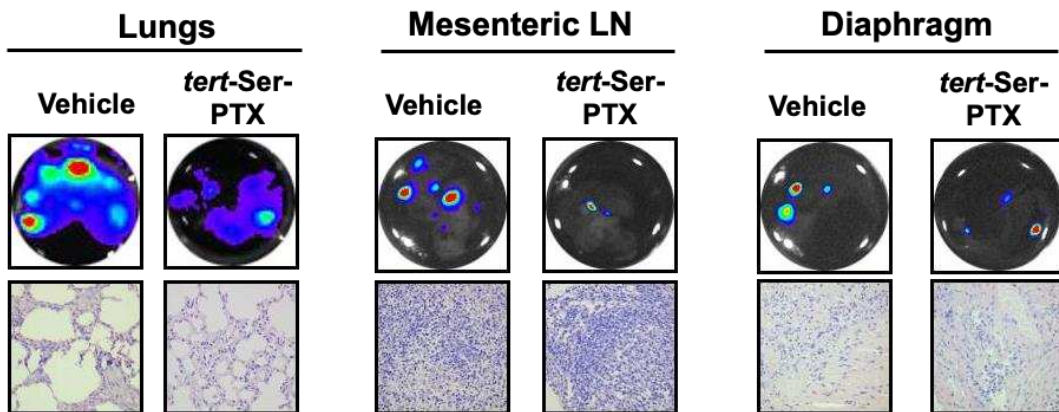


Figure 8. Effect of *tert*-Ser-PTX treatment on distant metastasis in orthotopic LNCaP.Fluc2 prostate tumor-bearing mice. At the study endpoint, *ex vivo* BLI of excised lungs lymph nodes (perirenal, mesenteric, and peripancreatic) and diaphragm allowed the identification and localization of spontaneous hematologic (lung), lymphatic (lymph nodes), and coelomic (diaphragm) metastases. **a)** *ex vivo* bioluminescent quantification of metastasis and **b)** comparisons of bioluminescence and histopathology of different tissues of LNCaP.Fluc2 bearing mouse treated with 15 mg kg⁻¹ of *tert*-Ser-PTX and vehicle control. The significance threshold was established at $p < 0.05$, and significance levels were schematically assigned * ($0.01 \leq p < 0.05$), ** ($0.001 \leq p < 0.01$), *** ($0.0001 \leq p < 0.001$) or **** ($p < 0.0001$).

1 Furthermore, *tert*-Ser-PTX treatment reduced levels of distant hematological dissemination
2 to lungs, locoregional lymphatic dissemination to perirenal, mesenteric, and peripancreatic
3 lymph nodes, and coelomic dissemination to the diaphragm, as measured as incidence (**Table**
4 **S4**) or by BLI (**Figure 8**). We observed a statistically significant reduction ($p=0.0143$) in distant
5 hematological (lung metastases) dissemination and growth of LNCaP.Fluc2 PCa cells in *tert*-Ser-
6 PTX polymers compared to vehicle control treated-group (**Figure 8a**, first two columns). We also
7 found a T/C ratio of bioluminescent lung metastases growth of 8% for the *tert*-Ser-PTX treated
8 group. Furthermore, *ex vivo* BLI and histopathological images of spontaneous orthotopic
9 metastatic lesions from a representative mouse from each treatment schedule demonstrated
10 reduced metastasis growth following *tert*-Ser-PTX treatment (**Figure 8b**).
11
12
13
14
15
16
17

18 As for locoregional metastasis to lymph nodes and diaphragm, *ex vivo* BLI analysis
19 demonstrated a significant reduction in metastatic colonization of the lymph nodes ($p=0.0004$
20 for peripancreatic lymph nodes and $p<0.0001$ for perirenal and mesenteric lymph nodes) and
21 the diaphragm ($p=0.0001$), indicating that *tert*-Ser-PTX inhibits both lymphatic and coelomic
22 dissemination (**Figure 8a**). Interestingly, we noted greater inhibition of lymphatic and coelomic
23 metastasis than hematologic (lung) metastasis. The inhibition of dissemination and growth of
24 lymphatic metastasis is highly relevant in PCa, as 14% of metastases locate in the locoregional
25 lymph nodes.^[46] Unfortunately, the orthotopic prostate model employed does not readily
26 metastasize to the bone, which has an incidence of 65% in PCa,^[46] and, therefore, we could not
27 evaluate the impact of *tert*-Ser-PTX treatment on bone metastases.
28
29
30
31
32
33
34
35
36

37 We do note that we cannot exclude that the inhibition of primary tumor growth by *tert*-
38 Ser-PTX indirectly limited the growth of the metastatic foci; however, studies have established
39 that metastasis may develop in parallel with the development of the primary tumor, indicating
40 early tumor cell dissemination.^[47] Therefore, significant inhibition in local and distant metastasis
41 might suggest the direct impact of *tert*-Ser-PTX on metastatic foci. Nonetheless, the EPR effect
42 may not occur in metastases as in the primary tumor due to the lack of the angiogenic switch
43 and the lack of macromolecule accumulation at metastatic sites,^[48] suggesting that EPR does not
44 control *tert*-Ser-PTX efficacy on metastatic lesions.
45
46
47
48
49
50
51

52 With the EPR effect excluded, we hypothesize that the direct impact of *tert*-Ser-PTX could
53 be driven by the inhibitory effect of PTX on the vascular system^[14–16] and/or the potential
54 effectiveness of drug delivery systems on cancer stem cells (CSCs).^[48] CSCs may be responsible
55 for metastasis formation,^[50] and some drug delivery systems appear to overcome the inherent
56 chemoresistance of CSCs.^[49,51] This fact could justify the significant reduction in metastasis
57 incidence and growth in *tert*-Ser-PTX treated mice. Moreover, microtubule-binding drugs such
58
59
60
61
62
63
64
65

1 as PTX directly affect endothelial cells, and neoangiogenic tumor vessels by extension, at low
2 PTX concentrations. Therefore, the slow release of PTX from *tert*-Ser-PTX polymers may increase
3 anti-angiogenic activity.^[15,16] Indeed, the delivery of PTX in endothelially-targeted nanosystems
4 can increase PTX efficacy.^[52]
5

6
7 Regardless of the precise mechanism of action, we highlight the effectiveness of *tert*-Ser-
8 PTX in reducing distant and locoregional metastasis and inhibiting the growth of primary
9 orthotopic LNCaP. Fluc2 prostate tumors. Overall, our results demonstrate the potential of *tert*-
10 Ser-PTX in the treatment of PCa.
11
12
13
14
15

16 CONCLUSIONS

17
18 In this study, we report the development of a potentially effective PCa treatment via the
19 conjugation of a known chemotherapeutic agent Paclitaxel (PTX) to a biodegradable polyacetal
20 polymer. Polymer conjugation increases stability in circulation, inhibits off-target drug effects,
21 and promotes tumor accumulation via the EPR effect. Once internalized within PCa cells, the
22 alteration in pH mediates ester bond cleavage and PTX release together with polyacetal
23 mainchain degradation. *In vivo* toxicity and efficacy profiles of *tert*-Ser-PTX suggest robust anti-
24 tumor improvements compared to treatment with the standard formulations of PTX. Contrary
25 to free PTX, we found that *tert*-Ser-PTX was well tolerated after 11 doses at 15 mg PTX kg⁻¹ with
26 no adverse effects observed during the treatment period. Significantly, *tert*-Ser-PTX inhibited
27 orthotopic prostate LNCaP tumor growth and significantly reduced metastatic incidence.
28 Overall, this study highlights the potential of polyacetal conjugation as an improved strategy for
29 the delivery of chemotherapeutic drugs.
30
31
32
33
34
35
36
37
38
39
40
41
42
43

44 ACKNOWLEDGEMENTS

45
46 The authors would like to thank Richard M. England and Gabriela Rodriguez for experimental
47 support and Stuart P. Atkinson for English editing. This study was supported by grants from
48 CIBER-BBN (NanoMets Intramural Grant), "Fondo de Investigaciones Sanitarias - Instituto de
49 Salud Carlos III" (FIS-ISCIII) (PI14/02079 to SS), Spanish Ministry of Science and Innovation
50 (MICINN, IPT- 090000-2010-0001 to IA, IPT-2012-0712-010000 to MJV), MINECO (SAF2013-
51 44848-R, SAF2016-80427-R, and PID2019-108806RB-I00 to MJV), and the Valencian Council for
52 Innovation, Universities, Science and Digital Society (PROMETEO/2016/103 to MJV). The study
53 was co-funded by FEDER, ASEICA, and "Fundació Marató TV3" (PENTRI project 337/C/2013 to
54 IA) and SGR (2017 SGR 00638). The Spanish Ministry of Science and Innovation supported NG-A
55
56
57
58
59
60

(PTA2013-8431-I) and SM (PTA2013-8849-I) as laboratory technicians. The Science and Technology Facilities Council (STFC) is acknowledged for access to ILL and award of beamtime (9-13-504). SINTEF (SB, AH) and Trinity College (APM, AB, OLG) were supported by the EC as part of the European Nanomedicine Characterisation Laboratory (EUNCL) H2020 project (Grant no. 654190). Part of the equipment employed in this work has been funded by Generalitat Valenciana and co-financed with FEDER funds (PO FEDER of Comunitat Valenciana 2014–2020).

REFERENCES

- [1] L. Wan, K. Pantel, Y. Kang, *Nat. Med.* **2013**, *19*, 1450.
- [2] H. Sung, J. Ferlay, R. L. Siegel, M. Laversanne, I. Soerjomataram, A. Jemal, F. Bray, *CA. Cancer J. Clin.* **2021**, *71*, 209.
- [3] C. H. Pernar, E. M. Ebot, K. M. Wilson, L. A. Mucci, *Cold Spring Harb. Perspect. Med.* **2018**, *8*, a030361.
- [4] R. J. Rebello, C. Oing, K. E. Knudsen, S. Loeb, D. C. Johnson, R. E. Reiter, S. Gillessen, T. Van der Kwast, R. G. Bristow, *Nat. Rev. Dis. Prim.* **2021**, *7*, 9.
- [5] M. D. Shelley, S. Kumar, B. Coles, T. Wilt, J. Staffurth, M. D. Mason, *Cancer Treat. Rev.* **2009**, *35*, 9.
- [6] G. Attard, C. Parker, R. A. Eeles, F. Schröder, S. A. Tomlins, I. Tannock, C. G. Drake, J. S. De Bono, *Lancet* **2016**, *387*, 70.
- [7] S. Vicente-Ruiz, A. Serrano-Martí, A. Armiñán, M. J. Vicent, *Adv. Ther.* **2021**, *4*, 2000136.
- [8] R. Duncan, *Nat. Rev. Cancer* **2006**, *6*, 688.
- [9] H. Maeda, J. Wu, T. Sawa, Y. Matsumura, K. Hori, *J. Control. Release* **2000**, *65*, 271.
- [10] R. Duncan, R. Gaspar, *Mol. Pharm.* **2011**, *8*, 2101.
- [11] R. Tomlinson, M. Klee, S. Garrett, J. Heller, R. Duncan, S. Brocchini, *Macromolecules* **2002**, *35*, 473.
- [12] R. Tomlinson, J. Heller, S. Brocchini, R. Duncan, *Bioconjug. Chem.* **2003**, *14*, 1096.
- [13] V. Giménez, C. James, A. Armiñán, R. Schweins, A. Paul, M. J. Vicent, *J. Control. Release* **2012**, *159*, 290.
- [14] J. Wang, P. Lou, R. Lesniewski, J. Henkin, *Anticancer. Drugs* **2003**, *14*, 13.
- [15] J. R. Merchan, D. R. Jayaram, J. G. Supko, X. He, G. J. Bublely, V. P. Sukhatme, *Int. J. Cancer* **2005**, *113*, 490.
- [16] E. L. Schwartz, *Clin. Cancer Res.* **2009**, *15*, 2594.
- [17] H. Gelderblom, J. Verweij, K. Nooter, A. Sparreboom, *Eur. J. Cancer* **2001**, *37*, 1590.
- [18] R. da Costa, G. F. Passos, N. L. M. Quintão, E. S. Fernandes, J. R. L. C. B. Maia, M. M. Campos, J. B. Calixto, *Br. J. Pharmacol.* **2020**, *177*, 3127.
- [19] S. H. Jang, M. G. Wientjes, J. L. Au, *J. Pharmacol. Exp. Ther.* **2001**.
- [20] E. Miele, G. P. Spinelli, E. Miele, F. Tomao, S. Tomao, *Int. J. Nanomedicine* **2009**, *4*, 99.
- [21] K. Miller, R. Erez, E. Segal, D. Shabat, R. Satchi-Fainaro, *Angew. Chemie - Int. Ed.* **2009**, *48*, 2949.
- [22] C. J. Langer, K. J. O' Byrne, M. A. Socinski, S. M. Mikhailov, K. Leniewski-Kmak, M. Smakal, T. E. Ciuleanu, S. V Orlov, M. Dediu, D. Heigener, et al., *J. Thorac. Oncol.* **2008**, *3*, 623.
- [23] J. Zhao, E. J. Koay, T. Li, X. Wen, C. Li, *Wiley Interdiscip. Rev. Nanomed. Nanobiotechnol.* **2018**, *10(3)*, e1497.
- [24] L. Paz-Ares, H. Ross, M. O'Brien, A. Riviere, U. Gatzemeier, J. Von Pawel, E. Kaukel, L. Freitag, W. Digel, H. Bischoff, et al., *Br J Cancer* **2008**, *98*, 1608.
- [25] S. Lu, S. Y. Tsai, M. J. Tsai, *Cancer Res.* **1997**, *57*, 4511.
- [26] P. Botella, I. Abasolo, Y. Fernández, C. Muniesa, S. Miranda, M. Quesada, J. Ruiz, S. Schwartz, A. Corma, *J. Control. Release* **2011**, *156*, 246.
- [27] P. Rocas, Y. Fernandez, S. Schwartz, I. Abasolo, J. Rocas, F. Albericio, *J. Mater. Chem. B* **2015**, *3*, 7604.
- [28] L. L. Romero-Hernández, P. Merino-Montiel, S. Montiel-Smith, S. Meza-Reyes, J. L.

- Vega-Báez, I. Abasolo, S. Schwartz, Ó. López, J. G. Fernández-Bolaños, *Eur. J. Med. Chem.* **2015**, *99*, 67.
- [29] Y. Fernández, L. Forarada, N. García-Aranda, S. Mancilla, L. Suárez-López, M. V. Céspedes, J. R. Herance, D. Arango, R. Mangues, S. Schwartz, et al., *J. Mol. Biol. Mol. Imaging* **2015**, *2*, 1019.
- [30] J. Tian, V. J. Stella, *J. Pharm. Sci.* **2010**, *99*, 1288.
- [31] K. J. Volk, S. E. Hill, E. H. Kerns, M. S. Lee, *J. Chromatogr. B Biomed. Appl.* **1997**, *696*, 99.
- [32] F. Horkay, B. Hammouda, *Colloid Polym. Sci.* **2008**, *286*, 611.
- [33] Q. Peng, X.-Q. Wei, Q. Yang, S. Zhang, T. Zhang, X.-R. Shao, X.-X. Cai, Z.-R. Zhang, Y.-F. Lin, *Nanomedicine (Lond)*. **2015**, *10*, 205.
- [34] C. L. Oliveira, F. Veiga, C. Varela, F. Roleira, E. Tavares, I. Silveira, A. J. Ribeiro, *Colloids Surfaces B Biointerfaces* **2017**, *150*, 326.
- [35] S. A. Abouelmagd, B. Sun, A. C. Chang, Y. J. Ku, Y. Yeo, *Mol. Pharm.* **2015**, *12*, 997.
- [36] P. Gener, L. P. Gouveia, G. R. Sabat, D. F. de Sousa Rafael, N. B. Fort, A. Arranja, Y. Fernández, R. M. Prieto, J. S. Ortega, D. Arango, et al., *Nanomedicine Nanotechnology, Biol. Med.* **2015**, *11*, 1883.
- [37] E. M. Kemper, A. E. Van Zandbergen, C. Cleypool, H. A. Mos, W. Boogerd, J. H. Beijnen, O. Van Tellingen, *Clin. Cancer Res.* **2003**.
- [38] V. Omelyanenko, P. Kopecková, C. Gentry, J. Kopeček, in *J. Control. Release*, **1998**.
- [39] K. L. Hennenfent, R. Govindan, *Ann. Oncol.* **2006**, *17*, 735.
- [40] D.-W. Kim, S.-Y. S.-W. Kim, H.-K. Kim, S. W. Shin, J. S. Kim, K. Park, M. Y. Lee, D. S. Heo, *Ann. Oncol.* **2007**, *18*, 2009.
- [41] M. Qin, S. Peng, N. Liu, M. Hu, Y. He, G. Li, H. Chen, Y. He, A. Chen, X. Wang, *J. Pharmacol. Exp. Ther.* **2015**, *355*, 473.
- [42] B. Elsadek, R. Graeser, N. Esser, C. Schäfer-Obodozie, K. A. Ajaj, C. Unger, A. Warnecke, T. Saleem, N. El-Melegy, H. Madkor, et al., *Eur. J. Cancer* **2010**, *46*, 3434.
- [43] R. G. Lapidus, W. Dang, D. M. Rosen, A. M. Gady, Y. Zabelinka, R. O'Meally, T. L. DeWeese, S. R. Denmeade, *Prostate* **2004**, *58*, 291.
- [44] R. Yang, G. Mondal, D. Wen, R. I. Mahato, *Nanomedicine Nanotechnology, Biol. Med.* **2017**, *13*, 391.
- [45] R. A. Stephenson, C. P. N. Dinney, K. Gohji, N. G. Ordonez, J. J. Killion, I. J. Fidler, *J Natl Cancer Inst* **1992**.
- [46] K. R. Hess, G. R. Varadhachary, S. H. Taylor, W. Wei, M. N. Raber, R. Lenzi, J. L. Abbruzzese, *Cancer* **2006**, *106*, 1624.
- [47] C. A. Klein, *Nat. Rev. Cancer* **2009**, *9*, 302.
- [48] A. Schroeder, D. A. Heller, M. M. Winslow, J. E. Dahlman, G. W. Pratt, R. Langer, T. Jacks, D. G. Anderson, *Nat. Rev. Cancer* **2012**, *12*, 39.
- [49] P. Gener, D. F. de S. Rafael, Y. Fernández, J. S. Ortega, D. Arango, I. Abasolo, M. Videira, S. Schwartz, *Nanomedicine* **2016**, *11*, 307.
- [50] T. Brabletz, A. Jung, S. Spaderna, F. Hlubek, T. Kirchner, *Nat. Rev. Cancer* **2005**, *5*, 744.
- [51] Y. Zhou, J. Kopeček, *J. Drug Target.* **2013**, *21*, 1.
- [52] A. Eldar-Boock, K. Miller, J. Sanchis, R. Lupu, M. J. Vicent, R. Satchi-Fainaro, *Biomaterials* **2011**, *32*, 3862.

1
2
3 A biodegradable polyacetal-paclitaxel conjugate (*tert*-Ser-PTX), gained through robust
4 synthetic and analytical approaches, shows enhanced stability in human serum and
5
6 provides sustained release of PTX in a pH-responsive manner. *tert*-Ser-PTX significantly
7
8 reduced the systemic toxicities associated with free PTX treatment, effectively inhibited
9
10 primary tumor growth and hematologic, lymphatic, and coelomic dissemination in mice
11
12 carrying orthotopic Prostate Cancer tumors.
13
14
15

16
17
18 *Yolanda Fernández, Julie Movellan, Laia Foradada, Vanessa Giménez, Natalia García-Aranda,*
19 *Sandra Mancill^c, Ana Armiñán, Sven Even Borgos, Astrid Hyldbak^e, Anna Bogdanska, Oliviero L.*
20 *Gobbo, Adriele Prina-Mello, Jessica Ponti, Luigi Calzolari, Oleksandr Zagorodko, Elena Gallon*
21 *Amaya Niño-Pariente, Alison Paul, Simó Schwartz Jr., Ibane Abasolo* and María J. Vicent**
22
23
24
25
26
27

28
29 **In Vivo Anti-Tumor and Metastatic Efficacy Of A Polyacetal-Based Paclitaxel**
30
31 **Conjugate For Prostate Cancer Therapy**
32
33

